Published for SISSA by Springer
Received: April 28, 2023
Accepted: July 16, 2023
Published: August 2, 2023

Inclusive and multiplicity dependent production of electrons from heavy-flavour hadron decays in pp and p-Pb collisions

The ALICE collaboration

E-mail: alice-publications@cern.ch

Abstract: Measurements of the production of electrons from heavy-flavour hadron decays in pp collisions at $\sqrt{s} = 13\,\text{TeV}$ at midrapidity with the ALICE detector are presented down to a transverse momentum (p_T) of $0.2\,\text{GeV}/c$ and up to $p_\text{T} = 35\,\text{GeV}/c$, which is the largest momentum range probed for inclusive electron measurements in ALICE. In p-Pb collisions, the production cross section and the nuclear modification factor of electrons from heavy-flavour hadron decays are measured in the p_T range $0.5 < p_\text{T} < 26\,\text{GeV}/c$ at $\sqrt{s_\text{NN}} = 8.16\,\text{TeV}$. The nuclear modification factor is found to be consistent with unity within the statistical and systematic uncertainties. In both collision systems, first measurements of the yields of electrons from heavy-flavour hadron decays in different multiplicity intervals normalised to the multiplicity-integrated yield (self-normalised yield) at midrapidity are reported as a function of the self-normalised charged-particle multiplicity estimated at midrapidity. The self-normalised yields in pp and p-Pb collisions grow faster than linear with the self-normalised multiplicity. A strong p_T dependence is observed in pp collisions, where the yield of high-p_T electrons increases faster as a function of multiplicity than the one of low-p_T electrons. The measurement in p-Pb collisions shows no p_T dependence within uncertainties. The self-normalised yields in pp and p-Pb collisions are compared with measurements of other heavy-flavour, light-flavour, and strange particles, and with Monte Carlo simulations.

Keywords: Hadron-Hadron Scattering

ArXiv ePrint: 2303.13349

https://doi.org/10.1007/JHEP08(2023)006

JHEP08(2023)006

Contents

JHEP08(2023)006

1 Introduction

In high-energy hadronic collisions, heavy quarks are mainly produced in hard parton scattering processes. Due to their large masses, their production cross sections can be calculated in the framework of perturbative quantum chromodynamics (pQCD) down to low transverse momenta [1–4]. Measurements of production cross sections of open heavy-flavour hadrons and their decay products in pp and Pb-Pb collisions were performed by the ALICE, CMS, ATLAS and LHCb Collaborations at the LHC at both mid and forward rapidity [5–28]. These measurements are described by theoretical predictions based on pQCD calculations with the collinear factorisation approach at next-to-leading order with next-to-leading log resummation e.g. in the GM-VFNS (general-mass variable-flavour-number scheme) [29–33]) or the FONLL (fixed order with next-to-leading-log resummation) [34] frameworks, within theoretical uncertainties. Measurements of charm-baryon production

at midrapidity in pp collisions show an enhancement of the Λ_c^+/D^0 [14, 35–38], $\Xi_c^{+,0}/D^0$ [39–41], $\Sigma_c^{+,0}/D^0$ [42], and $\Omega_c^{+,0}/D^0$ [43] ratios with respect to those measured in e^+e^- and ep collisions [44]. A multiplicity dependence measurement of the Λ_c^+/D^0 ratio [14] has revealed a significant increase from the lowest to the highest multiplicity. These observations indicate that the hadronisation of charm quarks into charm hadrons is not a universal process among different collision systems. These findings are similar to those obtained in the beauty sector by the CDF Collaboration at the Tevatron [45] and by the LHCb Collaboration at the LHC [46, 47].

In proton-nucleus collisions, the so-called cold nuclear matter (CNM) effects occur due to the presence of a nucleus in the colliding system and to the large density of produced particles. In particular, the parton distribution functions (PDFs) of nucleons bound in nuclei are modified with respect to those of free nucleons, which can be described by phenomenological parameterisations referred to as nuclear PDFs (nPDFs) [48–51]. When the production process is dominated by gluons at low Bjorken-x, the nucleus can be described by the Colour Glass Condensate (CGC) effective theory as a coherent and saturated gluonic system [52–55]. The kinematics of the partons in the initial state can be affected by multiple scatterings [56, 57] or by gluon radiation (energy loss) before or after the heavy-quark pair is produced [58]. Measurements of heavy-flavour production in p-Pb collisions at the LHC will allow a study of the above mentioned effects. Previous measurements of the nuclear modification factor of leptons from heavy-flavour hadron decays in p-Pb collisions at $\sqrt{s_{\rm NN}} = 5.02\,\text{TeV}$ by the ALICE Collaboration indicate no significant modification of their yields due to CNM effects in the measured transverse momentum ($p_{\rm T}$) region within uncertainties [19, 59]. For a nucleus-nucleus collisions (AA), the nuclear modification factor ($R_{\rm AA}$) is the ratio of the yield in nucleus-nucleus collisions with respect to the yield in proton-proton collisions scaled by the number of binary nucleon-nucleon collision in AA. It quantifies the interaction of a particle and its energy loss while traversing through a medium formed in AA collisions with respect to pp collisions. Measurements of the nuclear modification factor of open heavy flavour and quarkonia at mid, forward, and backward rapidity in p-Pb collisions were performed by the ALICE [60–65], ATLAS [66], CMS [67, 68], and LHCb [69–72] collaborations. The results can be described qualitatively by the various theoretical calculations mentioned above.

Recent measurements of light-flavour [73–88] and heavy-flavour hadrons [89–93] in high-multiplicity pp, p-A, and d-A collisions at different energies have revealed strong flow-like effects in these small systems [94]. The origin of this phenomenon is debated. Models that incorporate hydrodynamical evolution of the system [95–98], overlapping strings [99], string percolation [100], or multiple-parton interactions together with colour reconnection [101, 102] can describe qualitatively the observed features in high-multiplicity events. A multiphase transport model [103], as well as calculations based on the fragmentation of saturated gluon states [104, 105], are also able to describe some features of the data. The measurement of heavy-flavour production in small systems as a function of the charged-particle multiplicity produced in the collision could thus provide further insight into the processes occurring in the collision at the partonic level and the interplay between the hard and soft mechanisms in particle production in pp and p-Pb collisions.

JHEP08(2023)006

Measurements of charm and beauty productions [106–111] indicate an increase of heavy-flavour production with charged-particle multiplicity measured at midrapidity. The D meson [106] and J/ψ [107] productions normalised to their corresponding multiplicity-integrated yields in minimum bias events (self-normalised yields), as a function of self-normalised event multiplicities, (i.e., normalised to the average multiplicity in minimum bias collisions) are measured in pp collisions at $\sqrt{s} = 7\,\text{TeV}$ and $\sqrt{s} = 13\,\text{TeV}$ by the ALICE Collaboration at the LHC, and at $\sqrt{s} = 0.2\,\text{TeV}$ by the STAR Collaboration at RHIC [108]. These measurements show a stronger than linear increase of self-normalised yields as a function of self-normalised multiplicity. Measurements of the Υ(nS) production in pp collisions at $\sqrt{s} = 2.76\,\text{TeV}$ and $\sqrt{s} = 7\,\text{TeV}$ by the CMS Collaboration at midrapidity indicate a linear increase with the event activity, when measuring it at forward rapidity, and a stronger than linear increase with the event activity measured at midrapidity [109]. A comprehensive review of the connection between the Υ(nS) production and the underlying event, is presented by the CMS Collaboration in pp collisions at $\sqrt{s} = 2.76\,\text{TeV}$ [112]. Measurements of multiplicity dependence of Υ(nS) production at forward rapidity, is presented by the ALICE Collaboration in pp collisions at $\sqrt{s} = 13\,\text{TeV}$ [113]. In p-Pb collisions, the self-normalised D meson yield at midrapidity increases with a faster than linear trend as a function of the self-normalised charged-particle multiplicity at midrapidity and is consistent with a linear growth for multiplicity measured at large rapidities [111]. The self-normalised J/ψ yield at larger rapidities also exhibits an increase with increasing normalised charged-particle pseudorapidity density, where the yield at backward rapidity grows faster than the forward rapidity one [110]. A possible correlation with the event multiplicity (and event shape) is also observed for the inclusive charged-particle production [114], and for identified particles, including multi-strange hyperons [115]. The trends are qualitatively, and for some of the calculations quantitatively, reproduced by QCD-inspired event generators such as PYTHIA 8 [116], and EPOS LHC and EPOS 3 [117, 118]. But a critical evaluation of the similarities and differences between the physics mechanisms at play in various models is yet to be performed. More stringent tests of the models would be important in this direction. A comparison of the multiplicity-dependent measurements for different particle species would also provide insight into the origin of the observed phenomena [14, 119].

In this article, measurements of the production cross section of electrons from heavy-flavour hadron decays at midrapidity in pp collisions at $\sqrt{s} = 13\,\text{TeV}$ and p-Pb collisions at $\sqrt{s_{\text{NN}}} = 8.16\,\text{TeV}$ are presented. The cross section of electrons from heavy-flavour hadron decays was measured as a function of transverse momentum down to $0.2\,\text{GeV}/c$ and up to $35\,\text{GeV}/c$ in pp collisions, which is the lowest and highest p_{T}-reach attained for electrons from heavy-flavour hadron decays with the ALICE detector. Results of the nuclear modification factor (R_{pPb}) of electrons from heavy-flavour hadron decays at midrapidity in p-Pb collisions at $\sqrt{s_{\text{NN}}} = 8.16\,\text{TeV}$ are reported as well. The self-normalised yields of electrons from heavy-flavour hadron decays measured for the first time as a function of charged-particle multiplicity estimated at midrapidity ($|\eta| < 1$) in pp and p-Pb collisions are also presented. The comparison of the self-normalised yields of electrons from heavy-flavour hadron decays with other particles measured using the ALICE detector and with Monte Carlo (MC) simulations is discussed.

JHEP08(2023)006

The article is structured as follows. In section 2, the ALICE apparatus, its main detectors and the data samples used for the analysis are reported. The definition of multiplicity and the calculation of the charged-particle pseudorapidity density is addressed in section 3. In section 4, the procedure employed to obtain the production cross sections of electrons from heavy-flavour hadron decays is explained. Section 5 describes the systematic uncertainties associated with the measurements. The results of the analysis are presented and discussed in section 6. Finally, the article is summarised in section 7.

2 Experimental apparatus and data sample

In LHC Run 2, the ALICE apparatus consisted of a central barrel, covering the pseudorapidity region $|\eta| < 0.9$, a muon spectrometer with $-4 < \eta < -2.5$ coverage, and forward- and backward-pseudorapidity detectors employed for triggering, background rejection, and event characterisation. A complete description of the detector and an overview of its performance are presented in refs. [94, 120, 121].

The central barrel detectors used in the analysis are the Inner Tracking System (ITS) [122], the Time Projection Chamber (TPC) [123], the Time-Of-Flight detector (TOF) [124, 125], and the Electromagnetic Calorimeters (EMCal and DCal) [126, 127]. They are embedded in a large solenoidal magnet that provides a magnetic field parallel to the beams axis. The ITS consists of six layers of silicon detectors, with the innermost two composed of Silicon Pixel Detectors (SPD). The ITS is used to reconstruct the primary vertex and to track charged particles. The TPC is the main tracking detector of the central barrel. It is a gas detector placed co-axially with the beam axis next to the ITS radially. It also enables charged-particle identification via the measurement of the particle specific energy loss ($\mathrm{d}E/\mathrm{d}x$) in the detector gas. The particle identification capabilities of the TPC are supplemented with the TOF detector, which provides a measurement of the time-of-flight of charged particles. The TOF is a gas detector which uses Multigap Resistive Plate Chamber (MRPC) [128] as its basic detecting element. The TOF detector has the capability to distinguish the electrons from pions, kaons, and protons up to $p_{\mathrm{T}} \approx 1\,\mathrm{GeV}/c$, $p_{\mathrm{T}} \approx 2.5\,\mathrm{GeV}/c$, and $p_{\mathrm{T}} \approx 4\,\mathrm{GeV}/c$, respectively. The EMCal and DCal detectors are shashlik-type sampling calorimeters consisting of alternate layers of lead absorber and scintillator material. The EMCal covers $|\eta| < 0.7$ in pseudorapidity and $\Delta\varphi = 107^\circ$ in azimuth. The DCal is located azimuthally opposite to the EMCal covering $0.22 < |\eta| < 0.7$ and $\Delta\varphi = 60^\circ$ plus $|\eta| < 0.7$ and $\Delta\varphi = 7^\circ$. In the following, EMCal and DCal will be together referred to as EMCal, as they are part of the same detector system. The smallest segmentation of the EMCal is a cell, which has a dimension of 6×6 cm^2 (0.0143 rad $\times$ 0.0143 rad) in its base placed in the $\eta \times \varphi$ direction. The electromagnetic calorimeters were used for electron identification and for triggering on rare events with high momentum particles in their acceptance.

The detectors at forward rapidity used in the analysis are the V0 [129] and T0 [129] detectors. The V0 detector, composed of two scintillator arrays placed on either side of the interaction point along the beam axis (with pseudorapidity coverage $2.8 < \eta < 5.1$ and $-3.7 < \eta < -1.7$), was utilised for triggering and for offline rejection of beam-

JHEP08(2023)006

induced background events. In p-Pb collisions, the contamination from beam-background interactions and electromagnetic interactions was further removed using the information from the Zero Degree Calorimeters (ZDC) [130] located at 112.5 m on both sides of the interaction point along the beam axis. The T0 detector, composed of two arrays of quartz Cherenkov counters, covers an acceptance of $4.6 < \eta < 4.9$ and $-3.3 < \eta < -3.0$, and is used to provide the start time for the TOF detector. The V0 and T0 detectors were also employed to determine the integrated luminosity.

The results presented in this article were obtained using data recorded by ALICE during the LHC Run 2 data taking periods between the years 2016 and 2018 for pp collisions at $\sqrt{s} = 13\,\text{TeV}$, and in 2016 for p-Pb collisions at $\sqrt{s_{\text{NN}}} = 8.16\,\text{TeV}$. While the nominal magnetic field used during the data taking is 0.5 T, for a subset of periods in pp collisions the magnetic field was reduced to 0.2 T (will be referred to as low-B field data set in the following sections), allowing for the measurement of electrons down to a p_{T} of 0.2 GeV/c. In p-Pb collisions, a centre-of-mass energy per nucleon-nucleon collision of $\sqrt{s_{\text{NN}}} = 8.16\,\text{TeV}$ was obtained by delivering proton and lead beams with energies of 6.5 TeV and 2.56 TeV per nucleon, respectively. Due to this asymmetry of the beam energy per nucleon, the proton-nucleon centre-of-mass rapidity frame is shifted by $\Delta y = 0.465$ in the direction of the proton beam.

Events used in the analyses were obtained using the minimum bias (MB) trigger provided by the V0 detector, and two single shower triggers based on the energy deposited in the EMCal [121, 131]. The MB trigger condition requires coincident signals in both scintillator arrays of the V0 detector. The EMCal trigger is based on the sum of energy in a sliding window of 4×4 cells above a given threshold. The energy thresholds of the two EMCal triggers were set to 4 GeV (EG2) and 9 GeV (EG1) for the pp data sets, and 5.5 GeV (EG2) and 8 GeV (EG1) for the p-Pb data sets.

In order to obtain a uniform acceptance of the detectors, only events with a reconstructed primary vertex within ± 10 cm from the centre of the detector along the beam line (z_{vtx}) were considered for both pp and p-Pb collisions. The number of selected events in pp and p-Pb collisions for different triggers, and the corresponding integrated luminosities [132, 133] are listed in table 1. In-bunch pileup events, where more than one collision occurs in the same bunch crossing and are recorded as a single event, were rejected using an algorithm based on track segments reconstructed with the SPD to detect multiple primary vertices. Out-of-bunch pileup events, where one or more collisions occur in bunch crossings different from the one that triggered the data acquisition, were then rejected based on the timing information provided by the V0 detector.

3 Multiplicity definition and corrections

The production of electrons from heavy-flavour hadron decays was investigated as a function of charged-particle pseudorapidity density ($\mathrm{d}N_{\text{ch}}/\mathrm{d}\eta$) in pp and p-Pb collisions. The $\mathrm{d}N_{\text{ch}}/\mathrm{d}\eta$ was measured in the pseudorapidity range $|\eta| < 1$. It was evaluated using the number of tracklets ($N_{\text{tracklets}}$) in the SPD [134, 135], defined as track segments pointing to the primary vertex and formed by joining pairs of hits in the two SPD layers.

JHEP08(2023)006

	pp $\sqrt{s} = 13$ TeV				p-Pb $\sqrt{s_{\rm NN}} = 8.16$ TeV		
Magnetic field (T)	0.2	0.5			0.5		
Trigger	MB	MB	EG2	EG1	MB	EG2	EG1
Number of events (10^6)	438	1755	116	96	39	0.6	3.4
Luminosity (nb^{-1})	7.6	30.3	811.3	8214.5	0.0190	0.0860	1.65
	$\pm$0.2	$\pm$0.7	$\pm$30.7	$\pm$378.7	$\pm$0.0005	$\pm$0.0025	$\pm$0.05

Table 1. Number of selected events in pp and p-Pb collisions for different triggers, and the corresponding integrated luminosities and their uncertainties.

The number of raw tracklets ($N_{\rm tracklets}$) in an event were corrected ($N^{\rm corr}_{\rm tracklets}$) for the variation of the detector conditions with time (fraction of active SPD channels) and its limited acceptance as a function of $z_{\rm vtx}$ using a data-driven event-by-event correction, following the procedure discussed in refs. [136]. The corrections were done by applying a $z_{\rm vtx}$ and time-dependent correction factor such that the measured average multiplicity is equalised to a reference value, which was chosen to be the largest mean SPD tracklet multiplicity observed over time. The correction factor for each event was randomly smeared using a Poisson distribution to take into account event-by-event fluctuations. The number of events, sliced in $N^{\rm corr}_{\rm tracklets}$ intervals, were corrected for the trigger and primary vertex finding efficiencies, following the procedure discussed in [107]. The former was estimated from MC simulations and the latter with a data-driven approach. The efficiencies were close to unity for all multiplicity classes except for the lowest multiplicity class interval, where the efficiency was close to 90%.

Detector inefficiencies, production of secondary particles due to interactions with the detector material, and particle decays give a different number of reconstructed tracklets compared to the true primary charged-particle multiplicity value $N_{\rm ch}$ [137]. MC simulations using the PYTHIA 8.2 [116] and the DPMJET [138] event generators, for pp and p-Pb collisions respectively, and the GEANT 3 [139] transport code were used to estimate $N_{\rm ch}$ from $N^{\rm corr}_{\rm tracklets}$ and later $\mathrm{d}N_{\rm ch}/\mathrm{d}\eta$. A second-order polynomial correlation was assumed between the two quantities, $N_{\rm ch}$ and $N^{\rm corr}_{\rm tracklets}$, for the full $N^{\rm corr}_{\rm tracklets}$ range. To estimate the systematic uncertainties on $\mathrm{d}N_{\rm ch}/\mathrm{d}\eta$, possible deviations from the second-order polynomial correlation between $N_{\rm ch}$ and $N^{\rm corr}_{\rm tracklets}$ were estimated using a linear function. The systematic uncertainty on the residual $z_{\rm vtx}$ dependence due to differences between data and MC amounts to about 1% in pp collisions and is negligible in p-Pb collisions. The total systematic uncertainty on $\mathrm{d}N_{\rm ch}/\mathrm{d}\eta$ is about 5% in all multiplicity intervals for both pp and p-Pb collisions.

The average charged-particle pseudorapidity density was normalised to its average value in INEL > 0 events in pp and p-Pb collisions. The INEL > 0 event class contains all events with at least one charged particle within $|\eta| < 1$. The average charged-particle pseudorapidity densities ($\langle \mathrm{d}N_{\rm ch}/\mathrm{d}\eta \rangle$) for INEL > 0 were found to be in agreement with the previous published ALICE measurements [107, 110, 140]. The resulting values of the self-normalised charged-particle pseudorapidity density ($\mathrm{d}N_{\rm ch}/\mathrm{d}\eta / \langle \mathrm{d}N_{\rm ch}/\mathrm{d}\eta \rangle$) for the event classes considered in the analyses presented here are summarised in table 2.

JHEP08(2023)006

	pp $\sqrt{s} = 13$ TeV		p-Pb $\sqrt{s_{\rm NN}} = 8.16$ TeV	
Multiplicity class	$N^{\rm corr}_{\rm tracklets}$	$\mathrm{d}N_{\rm ch}/\mathrm{d}\eta/\langle \mathrm{d}N_{\rm ch}/\mathrm{d}\eta\rangle$	$N^{\rm corr}_{\rm tracklets}$	$\mathrm{d}N_{\rm ch}/\mathrm{d}\eta/\langle \mathrm{d}N_{\rm ch}/\mathrm{d}\eta\rangle$
I	1–14	0.48	1–38	0.51
II	15–24	1.63	39–55	1.32
III	25–34	2.50	56–95	2.03
IV	35–44	3.34	96–121	3.01
V	45–54	4.16	122–300	3.85
VI	55–64	4.97		
VII	65–120	6.05		

Table 2. Average self-normalised charged-particle pseudorapidity density ($\mathrm{d}N_{\rm ch}/\mathrm{d}\eta/\langle \mathrm{d}N_{\rm ch}/\mathrm{d}\eta\rangle$) in $|\eta| < 1.0$ for each event class selected in pp and p-Pb collisions.

4 Analysis overview

Measurements of electrons from heavy-flavour hadron decays were obtained by selecting an inclusive electron sample and subtracting electrons which do not originate from heavy-flavour hadron decays. The measurements were performed by identifying electrons using the TPC and TOF detectors at low $p_{\rm T}$ ($p_{\rm T} < 4$ GeV/c) and the TPC and EMCal detectors at higher $p_{\rm T}$ ($p_{\rm T} > 3$ GeV/c) offering the largest $p_{\rm T}$ reach. In particular, this ensures that the systematic uncertainties and the hadron contamination are small over the whole transverse momentum range. In the interval $3 < p_{\rm T} < 4$ GeV/c, where the heavy-flavour decay electron production was measured with both techniques, the TPC-TOF analysis was used for the final results, while the TPC-EMCal analysis was utilised as a consistency check. This choice was motivated by the precision of the measurements based on the statistical and systematic uncertainties, as will be further discussed in section 6. Throughout the article, the term 'electron' is used for electrons and positrons.

4.1 Electron identification

Reconstructed tracks were selected based on the criteria listed in table 3, which are similar to those used in the analysis described in [141, 142]. These requirements were applied depending on the data sample as well as the transverse momentum region of the analysis. The rapidity ranges used in the nominal-B field TPC-TOF analysis and the TPC-EMCal analysis were limited to $|y| < 0.8$ and $|y| < 0.6$, respectively, to avoid the edges of the detectors, where the systematic uncertainties related to the particle identification increase. In the low-B field TPC-TOF analyses for pp collisions, the rapidity interval was restricted to $|y| < 0.5$, to ensure a stable estimation of the photonic electron background (section 4.2), which significantly increases in the low-B field sample for small $p_{\rm T}$ and large rapidities, resulting in a small signal over background ratio. A charged particle passing through the TPC deposits energy inducing signals in the pad rows of the detector. The reconstructed

JHEP08(2023)006

space points are known as clusters. The number of crossed rows which is equivalent to the effective cluster track length is used as a criteria for selecting tracks. A threshold of a minimum of 70 out of the total 159 crossed rows of the TPC for track reconstruction and 80 clusters for particle identification were used. The χ^2 of the Kalman fit of the reconstructed track in the TPC, normalised to the number of TPC clusters ($\chi^2/N_{\mathrm{TPC}}^{\mathrm{cls}}$), had to be smaller than 4 to select tracks with good quality and reduce the contribution from wrongly attached clusters to the reconstructed track. Only tracks with a distance of closest approach (DCA) to the primary vertex smaller than 1 cm in the transverse plane and 2 cm in the longitudinal direction were selected in order to reject background and non-primary tracks. In the TPC-TOF analyses, all tracks were required to have an associated hit in each of the two innermost layers of the ITS to reduce the background electrons from photon conversions in the material, and to reduce wrong assignations of hits in the first layer of the ITS. For the TPC-EMCal analyses, the tracks were required to have at least one hit in one of the two innermost layers of the ITS. This reduces the impact of the inactive channels in the first ITS layer in the acceptance window of the EMCal. As the photon conversion background decreases with increasing p_{T}, the relaxed requirement does not affect the signal over background ratio significantly in the p_{T} range where the TPC-EMCal analyses were performed. Moreover, it is important to note that the track selection criteria on SPD, TOF, and EMCAL detectors sufficiently suppress background tracks originating from out-of-bunch pileup.

To identify electrons at low p_{T} ($p_{\mathrm{T}} < 4\,\mathrm{GeV}/c$), the specific energy deposition ($\mathrm{d}E/\mathrm{d}x$) in the TPC and the time-of-flight measurement in the TOF detector were used. The discriminant variable used for the TPC (TOF) detector is the deviation of $\mathrm{d}E/\mathrm{d}x$ (particle time-of-flight) from the parameterised electron Bethe-Bloch (electron time-of-flight) expectation value [143], expressed in terms of the $\mathrm{d}E/\mathrm{d}x$ (time-of-flight) resolution, $n_{\sigma,\mathrm{e}}^{\mathrm{TPC}}$ ($n_{\sigma,\mathrm{e}}^{\mathrm{TOF}}$). In the left panel of figure 1, $n_{\sigma,\mathrm{e}}^{\mathrm{TPC}}$ is shown as a function of the momentum of the track (p) after TOF selection. For $0.2 < p_{\mathrm{T}} < 4\,\mathrm{GeV}/c$, electron candidates were selected by requiring $|n_{\sigma,\mathrm{e}}^{\mathrm{TOF}}| < 3$ and $-1 < n_{\sigma,\mathrm{e}}^{\mathrm{TPC}} < 3$, resulting in a 100% pure electron sample at $p_{\mathrm{T}} \approx 0.2$ GeV/c, and a sample with a purity of about 90% at 4 GeV/c. The remaining hadron contamination in the sample, after TOF selection, was estimated and subtracted by parameterising the TPC $\mathrm{d}E/\mathrm{d}x$ distribution for each particle species with an analytical function in different momentum regions as shown in the right panel of figure 1, and as performed in previous analyses [141, 142].

Analyses using TPC and EMCal detectors were performed by spatially matching reconstructed charged tracks in the ITS and TPC with EMCal clusters. This is implemented by extrapolating the reconstructed charged tracks with ITS and TPC to the EMCal, taking into account the energy loss of the particle when it traverses the detector materials, and matching within the $\Delta\eta$ and $\Delta\varphi$ as given by eq. (4.1). At low p_{T}, the position resolution of tracks and the EMCal clusters gets worse which leads to a p_{T}-dependent matching criteria. The p_{T}-dependent selection window is approximately one EMCal cell size at high p_{T} and few cell sizes below 1 GeV/c [131]. This matching criterion removes the contribution from

JHEP08(2023)006

	pp $\sqrt{s} = 13$ TeV			p-Pb $\sqrt{s_{\mathrm{NN}}} = 8.16$ TeV	
p_{T} interval (GeV/c)	0.2–4.0	0.5–4.0	3.0–35.0	0.5–4.0	3.0–26.0
Track selection criteria	Low-B TPC-TOF	Nominal-B TPC-TOF	Nominal-B TPC-EMCal	Nominal-B TPC-TOF	Nominal-B TPC-EMCal
$\lvert y \rvert$	< 0.5	< 0.8	< 0.6	< 0.8	< 0.6
No. of TPC crossed rows	≥ 70	≥ 70	≥ 70	≥ 70	≥ 70
No. of TPC dE/dx clusters for PID	≥ 80	≥ 80	≥ 80	≥ 80	≥ 80
Number of ITS hits	≥ 3	≥ 3	≥ 3	≥ 3	≥ 3
$\chi^2/N_{\mathrm{TPC}}^{\mathrm{cls}}$	< 4	< 4	< 4	< 4	< 4
Minimum number of hits in the SPD	2	2	1	2	1
$\lvert \mathrm{DCA_{xy}} \rvert$	< 1 cm	< 1 cm	< 1 cm	< 1 cm	< 1 cm
$\lvert \mathrm{DCA_{z}} \rvert$	< 2 cm	< 2 cm	< 2 cm	< 2 cm	< 2 cm

Table 3. Summary of the track selection criteria imposed on the inclusive electron candidates for different data sets and electron identification strategies. Details can be found in section 4.1.

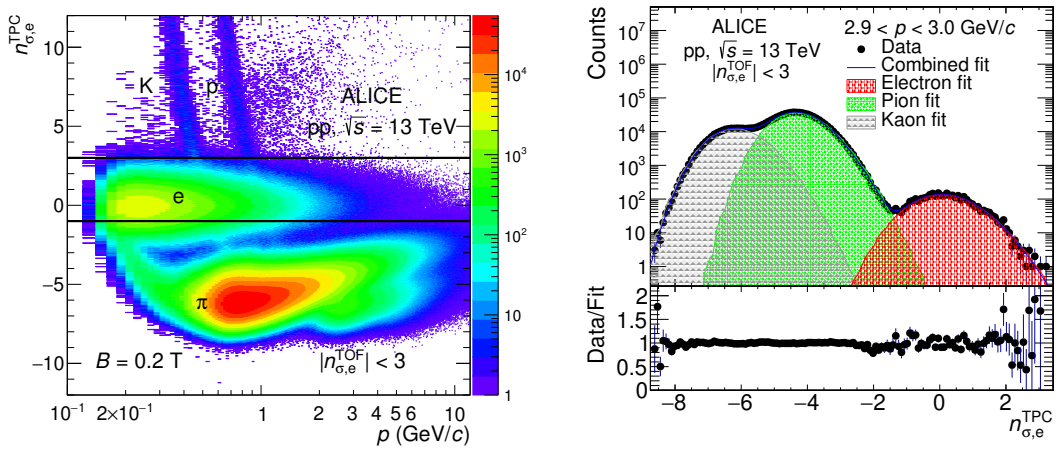

Figure 1. TPC dE/dx signal, expressed in terms of deviation from the expected electron energy loss as a function of momentum (left panel) and fit of the measured $n_{\sigma,\mathrm{e}}^{\mathrm{TPC}}$ distribution after the $n_{\sigma,\mathrm{e}}^{\mathrm{TOF}}$ requirement in the momentum range $2.9 < p < 3.0$ GeV/c (right panel) in pp collisions at $\sqrt{s} = 13$ TeV for the low-B field data set.

JHEP08(2023)006

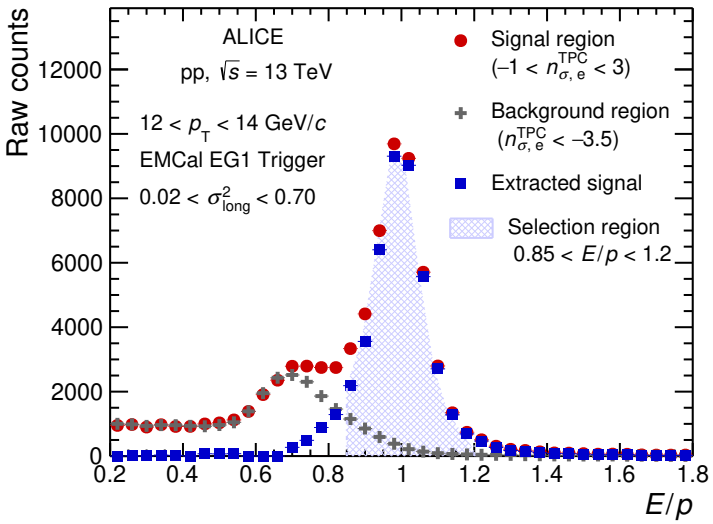

Figure 2. The E/p distribution measured in pp collisions at $\sqrt{s} = 13$ TeV for EG1 triggered events.

photon signals and from wrong associations of EMCal clusters to charged-particle tracks.

$$\begin{aligned} |\Delta\eta| &\leq 0.010 + (p_{\mathrm{T,track}}(\mathrm{GeV}/c) + 4.07)^{-2.5}, \\ |\Delta\varphi| &\leq 0.015 + (p_{\mathrm{T,track}}(\mathrm{GeV}/c) + 3.65)^{-2}. \end{aligned} \tag{4.1}$$

Candidate tracks matched with EMCal clusters with $-1 < n^{\mathrm{TPC}}_{\sigma,\mathrm{e}} < 3$ were selected. Electrons were identified and separated from hadrons using the E/p information, where, E is the energy deposited by the particle in the EMCal detector and p is the momentum of the track. It was required that the measured E/p is around unity, $0.85 < E/p < 1.2$, as expected for electrons, while hadrons have lower E/p values. To further reduce the amount of hadron contamination, a condition on the shape of the electromagnetic shower, σ^2_{long}, [144] was applied. The quantity σ^2_{long} stands for the eigenvalues of the dispersion matrix of the shower shape ellipse defined by the energy distribution within the EMCal cluster [145, 146]. A p_{T}-dependent selection criterion was applied, $0.02 < \sigma^2_{\mathrm{long}} < 0.9$ at low p_{T} and a more stringent selection up to $0.02 < \sigma^2_{\mathrm{long}} < 0.5$ at higher p_{T}, in both pp and p-Pb collisions. The lower threshold on σ^2_{long} removes contamination caused by neutrons hitting the readout electronics. The remaining hadron contamination in the electron sample was estimated by fitting the measured E/p distributions of electron candidates in momentum slices. For this purpose, the shape of the E/p spectrum for hadrons was obtained by selecting hadrons in the TPC with $n^{\mathrm{TPC}}_{\sigma,\mathrm{e}} < -3.5$. The obtained hadron E/p distribution was then scaled to match the E/p distribution of electron candidates in a region within $E/p < 0.7$, as shown in figure 2. The electron yield was calculated by integrating the E/p distributions of electron candidates in the range $0.85 < E/p < 1.2$ after the subtraction of the hadron contamination. In the pp (p-Pb) analysis, the hadron contamination was negligible at low p_{T}, increasing up to 23% (25%) at $p_{\mathrm{T}} = 35$ (26) GeV/c.

JHEP08(2023)006

4.2 Subtraction of electrons from non heavy-flavour sources

The selected inclusive electron sample contains electrons from open heavy-flavour hadron decays and from different sources of background:

- dielectrons originating from Dalitz decays of light-neutral mesons such as π^0, η as well as conversions of photons in the detector material, named as photonic electrons in the text,
- dielectrons from decays of J/ψ (J/$\psi \rightarrow e^+e^-$) and low-mass vector mesons ($\rho \rightarrow e^+e^-$, $\omega \rightarrow e^+e^-$, $\phi \rightarrow e^+e^-$),
- electrons from kaon weak decays $K^{0,\pm} \rightarrow e^{\pm}\, \pi^{\mp,0}\, \overset{(-)}{\nu}_e$ (K_{e3}),
- electrons from W and Z decays.

The dominant sources of background electrons are photon conversions in the detector material and Dalitz decays of light-neutral mesons. These contributions were estimated using an invariant mass technique [59] of electron-positron pairs. Unlike-signed electron-positron pairs (ULS) were defined by pairing the selected electrons with opposite-charge electron partners. To increase the efficiency of finding the partner, associated electrons were selected applying similar but looser track quality and particle identification criteria than those used for selecting signal electrons. The selection criteria are summarised in table 4. The electron-positron pairs from photonic background have a small invariant mass ($m_{e^+e^-}$). Heavy-flavour decay electrons can form ULS pairs mainly through random combinations with other electrons. The combinatorial contribution was estimated from the invariant mass distribution of like-signed electron (LS) pairs. The photonic background contribution was then evaluated by subtracting the LS distribution from the ULS one in the invariant mass region $m_{e^+e^-} < 0.14\,\mathrm{GeV}/c$. The efficiency of finding the partner electron, called tagging efficiency (ϵ_{tag}) from hereon, was estimated using MC simulations. In the pp and p-Pb analyses, the MC sample was obtained using PYTHIA 6 [116] and HIJING [147] generators, respectively. The generated particles were propagated through the ALICE apparatus using GEANT 3 [139]. In order to increase the statistical precision of ϵ_{tag} using the invariant mass method, π^0 and η mesons were embedded in the simulated events. The simulated π^0 and η p_{T} distributions were reweighted to match the measured spectra. For pp collisions, the π^0 spectrum was estimated as the average of the spectra of π^+ and π^- [148], whereas the η spectrum was obtained using m_{T} scaling, as in [149–151]. For the p-Pb analysis, the measured transverse momentum spectra of π^0 and η were used [152]. In the pp analysis, the tagging efficiency at low p_{T} ($p_{\mathrm{T}} < 1.0\,\mathrm{GeV}/c$) is 55–65% for the low-$B$ field data set, whereas for the nominal-B field data set it is around 45–55% at low p_{T} ($p_{\mathrm{T}} < 1.0\,\mathrm{GeV}/c$) increasing to about 85% at high p_{T} ($p_{\mathrm{T}} > 15\,\mathrm{GeV}/c$). In the p-Pb analysis, the tagging efficiency varies between 40% at low p_{T} ($p_{\mathrm{T}} < 3.0\,\mathrm{GeV}/c$) and 80% at high p_{T} ($p_{\mathrm{T}} > 7.0\,\mathrm{GeV}/c$).

Due to the requirement of hits in the SPD layers, the contribution of electrons from K_{e3} decays was found to be negligible with respect to the heavy-flavour signal for $p_{\mathrm{T}} > 0.5\,\mathrm{GeV}/c$. At lower p_{T}, the relative contribution of electrons from K_{e3} decays becomes non-negligible and hence it was subtracted from the p_{T}-differential cross section of electrons from

JHEP08(2023)006

	pp $\sqrt{s} = 13$ TeV			p-Pb $\sqrt{s_{\rm NN}} = 8.16$ TeV	
$p_{\rm T}$ interval (GeV/c)	0.2–4.0	0.5–4.0	3.0–35.0	0.5–4.0	3.0–26.0
Track and PID cuts	Low-B TPC-TOF	Nominal-B TPC-TOF	Nominal-B TPC-EMCal	Nominal-B TPC-TOF	Nominal-B TPC-EMCal
$p_{\rm T}^{\rm min}$	0.0 GeV/c	0.1 GeV/c	0.1 GeV/c	0.1 GeV/c	0.1 GeV/c
$\lvert y\rvert$	< 0.8	< 0.9	<0.9	< 0.8	< 0.8
No. of TPC dE/dx clusters for PID	≥ 60	≥ 60	≥ 60	≥ 60	≥ 60
Number of ITS hits	≥ 2	≥ 2	≥ 2	≥ 2	≥ 2
$\chi^2/N_{\rm TPC}^{\rm cls}$	< 4	< 4	< 4	< 4	< 4
$\lvert{\rm DCA_{xy}}\rvert$	< 1 cm	< 1 cm	< 1 cm	< 1 cm	< 1 cm
$\lvert{\rm DCA_{z}}\rvert$	< 2 cm	< 2 cm	< 2 cm	< 2 cm	< 2 cm

Table 4. Summary of the track selection criteria imposed on the associated electron candidates for different data sets and electron identification strategies.

heavy-flavour hadron decays. The $\rm K_{e3}$ contribution was estimated using a parameterisation of the ratio of $\rm K_{e3}$ to photonic electrons obtained from previous analyses using the so-called cocktail approach [9, 153, 154]. The same parametrisation was used in the analysis of pp collisions at $\sqrt{s} = 13$ TeV and in p-Pb collisions at $\sqrt{s_{\rm NN}} = 8.16$ TeV.

Other background contributions of $\rm e^+e^-$ pairs from J/ψ and low-mass vector mesons were negligible [153, 155] compared to the signal and were therefore not subtracted. Electrons from $\rm W^{\pm}$ and $\rm Z^0$ boson decays form a significant background at high $p_{\rm T}$ ($p_{\rm T} > 20$ GeV/c), which was estimated with the next-to-leading order event generator POWHEG [156], interfaced with PYTHIA as a decayer, and subtracted from the $p_{\rm T}$-differential cross section of electrons from heavy-flavour hadron decays. This contribution increases from 1% at $p_{\rm T} = 15$ GeV/c to about 3% at $p_{\rm T} = 20$ GeV/c and up to 25% at $p_{\rm T} = 35$ GeV/c with respect to the heavy-flavour decay electron yield in both pp and p-Pb collisions.

In pp collisions, the ratio of signal over background electrons is about 0.08 at $p_{\rm T} = 0.2$ GeV/c, 3 at $p_{\rm T} = 0.5$ GeV/c increasing to ~ 10.5 at $p_{\rm T} = 25$ GeV/c and reaches 12.3 at $p_{\rm T} = 35$ GeV/c, whereas in p-Pb collisions it is about 2.65 at $p_{\rm T} = 0.5$ GeV/c and increases up to 8.39 at $p_{\rm T} = 26$ GeV/c.

4.3 EMCal trigger rejection factor

The EMCal triggered events are reported in terms of $N_{\rm evt} \times {\rm RF}$, where $N_{\rm evt}$ is the number of triggered collisions and the Rejection Factor (RF) is the average number of rejected MB

JHEP08(2023)006

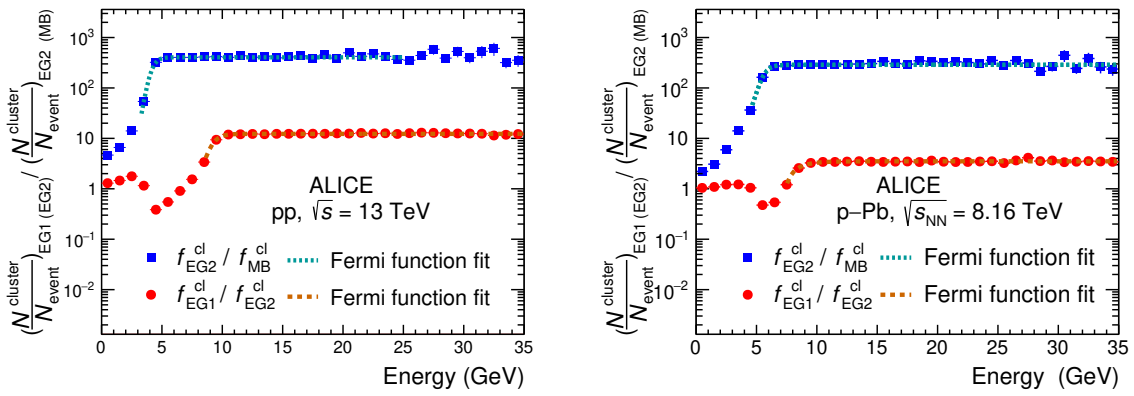

Figure 3. Trigger RF for EG2 and EG1 triggers in pp collisions at $\sqrt{s} = 13$ TeV (left panel) and in p-Pb collisions at $\sqrt{s_{NN}} = 8.16$ TeV (right panel).

	pp $\sqrt{s} = 13$ TeV		p-Pb $\sqrt{s_{NN}} = 8.16$ TeV	
Trigger	EG2	EG1	EG2	EG1
RF value	406	4985	283.4	1020.7
	± 1 (stat.) ± 12 (syst.)	± 11 (stat.) ± 200 (syst.)	± 1.5 (stat.) ± 5.9 (syst.)	± 3.6 (stat.) ± 30.4 (syst.)

Table 5. Multiplicity-integrated values of the EMCal trigger RF with their uncertainties for the EG2 and EG1 triggered data sets in pp and p-Pb collisions.

events per EMCal triggered event. The RFs were estimated with a data-driven method. For the EG2 trigger the RF was calculated as the ratio of the cluster energy distribution in EG2 triggered data to the one in MB triggered data (f^{cl}_{EG2}/f^{cl}_{MB}), which gives the EG2 turn-on curve. In order to reduce the effect of poor statistics in the MB sample at high p_T, the EG1 trigger turn-on curve was obtained using the ratio of the EG1 triggered data cluster energy distribution to the one in EG2 triggered data ($f^{cl}_{EG1}/f^{cl}_{EG2}$). The RF of EG1 trigger is then the product of f^{cl}_{EG2}/f^{cl}_{MB} and $f^{cl}_{EG1}/f^{cl}_{EG2}$. The turn-on curve was determined for the multiplicity-integrated interval and for different multiplicity intervals in pp and p-Pb collisions. The turn-on curves are shown for both trigger energy thresholds (EG1 and EG2) in multiplicity integrated pp and p-Pb collisions in figure 3.

A Fermi function [157, 158] was used to fit the trigger turn-on curves and determine the RF above the trigger threshold. The fit range is from the beginning of the turn-on region i.e. near trigger threshold to the highest energy where the distribution remains flat. The EG2/MB and the EG1/EG2 values correspond to the constant values determined by the plateau of the fitted Fermi function above the trigger thresholds. The final values of the RF used in the analyses are summarised in table 5. The systematic uncertainty on the trigger RF was estimated by varying the fit region of the trigger turn-on curve and the fit function, i.e. using a linear function in the plateau region. A systematic uncertainty of 3% (2%) for the EG2 trigger and 4% (3%) for EG1 trigger was obtained for pp (p-Pb) collisions.

JHEP08(2023)006

4.4 Efficiency correction and normalisation

The raw number of electrons and positrons from heavy-flavour hadron decays, $N_{\rm raw}$, was obtained by subtracting the hadron contamination, photonic electrons, and the other background electron contributions. The $p_{\rm T}$-differential cross section of electrons from heavy-flavour hadron decays at midrapidity was then calculated using the formula

$$\frac{{\rm d}^2\sigma}{{\rm d}p_{\rm T}{\rm d}y} = \frac{1}{2}\frac{1}{\Delta y \Delta p_{\rm T}}\frac{N_{\rm raw}}{\epsilon^{\rm geo}\times\epsilon^{\rm reco}\times\epsilon^{\rm eID}}\frac{1}{\mathcal{L}_{\rm int}}\,, \tag{4.2}$$

where $\mathcal{L}_{\rm int}$ is the integrated luminosity, and $\Delta p_{\rm T}$ and Δy the width of the $p_{\rm T}$ and rapidity intervals, respectively. The integrated luminosity was calculated using the number of analysed events and the measured MB trigger cross sections ($\sigma_{\rm MB}$), as $N_{\rm evt}/\sigma_{\rm MB}$ for minimum bias triggered events and $N_{\rm evt}\times{\rm RF}/\sigma_{\rm MB}$ for EMCal triggered events, and are listed in table 1. The trigger bias was studied in MC simulations and was found to be negligible for the selections applied to tracks and clusters. The measured $\sigma_{\rm MB}$ values are 58.44 ± 1.11 mb, 58.10 ± 1.57 mb, and 57.52 ± 1.21 mb for the pp collisions at $\sqrt{s} = 13$ TeV collected in the years 2016, 2017, and 2018, respectively [159], and 2100 ± 60 mb [133] in p-Pb collisions at $\sqrt{s_{\rm NN}} = 8.16$ TeV. The raw number of electrons from heavy-flavour hadron decays was corrected for the geometrical acceptance ($\epsilon^{\rm geo}$), the track reconstruction ($\epsilon^{\rm reco}$), and electron identification ($\epsilon^{\rm eID}$) efficiencies. The factor of two accounts for the charged averaged contribution of electrons and positrons. The trigger and event selection criteria were found to be fully efficient for electrons from heavy-flavour hadron decays.

The above mentioned acceptance and track reconstruction efficiencies are computed by means of MC simulations using PYTHIA 6 [116] and HIJING [147] event generators for pp and p-Pb collisions, respectively. For pp simulations PYTHIA 6 generated events with at least one $\rm c\overline{c}$ or $\rm b\overline{b}$ pair were selected for propagation through the apparatus with GEANT 3 [139] and subsequent reconstruction. In the case of p-Pb collisions, to have an efficient generation of heavy-flavour signals and reproduce the detector occupancy, one PYTHIA 6 event with a $\rm c\overline{c}$ or $\rm b\overline{b}$ pair was embedded in each HIJING simulated event.

The electron identification (eID) efficiencies for the TOF, TPC, and EMCal detectors were obtained separately, and then multiplied according to the detectors used in the analysis to compute the full electron identification efficiency $\varepsilon^{\rm eID}$. The TPC-TOF track matching and electron identification efficiency of the TOF detector was calculated with the above mentioned MC sample and was found to be 60–70% (40–65%) for $0.5 < p_{\rm T} < 1.5\,{\rm GeV}/c$ increasing up to 75% (70%) at $4\,{\rm GeV}/c$ in the low (nominal)-B field analysis. A better track matching between the TPC and the TOF detectors is achieved at a given $p_{\rm T}$ with the low-B field compared to the nominal-B field, due to the smaller curvature of the tracks. Therefore, a higher reconstruction efficiency is observed in the low-B field data compared to the nominal-B field sample. The TPC electron identification efficiency was determined using a data-driven approach based on the $n_{\sigma,{\rm e}}^{\rm TPC}$ distribution [9]. It is about 88% at $p_{\rm T} = 0.2\,{\rm GeV}/c$ and increases to 89% for $p_{\rm T} > 0.5\,{\rm GeV}/c$, for the low-$B$ field data sample.

In the nominal-B field data set, it was found to be around 86% at $p_{\rm T} = 0.5\,{\rm GeV}/c$ increasing to 88% for $p_{\rm T} > 4\,{\rm GeV}/c$. The electron identification efficiency with EMCal was estimated using MC simulations and was found to be about 60% at $3\,{\rm GeV}/c$, increasing up

JHEP08(2023)006

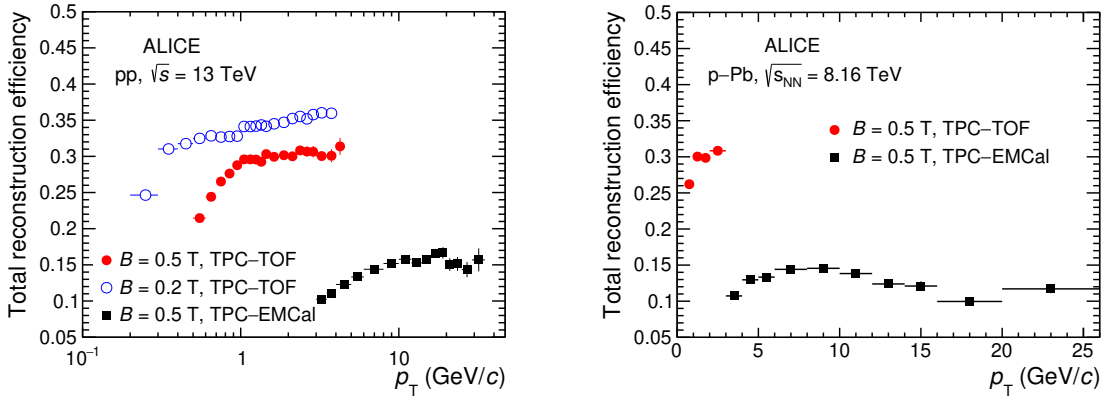

Figure 4. Total reconstruction efficiency of electrons from heavy-flavour hadron decays using the TPC and TOF or the TPC and EMCal detectors in pp collisions at $\sqrt{s} = 13\,\text{TeV}$ with nominal and low magnetic field (left panel) and in p-Pb collisions at $\sqrt{s_{\text{NN}}} = 8.16\,\text{TeV}$ (right panel).

to 80% for p_{T} larger than $10\,\text{GeV}/c$ for pp collisions. The total reconstruction efficiency ($\epsilon^{\text{geo}} \times \epsilon^{\text{reco}} \times \epsilon^{\text{eID}}$) for different data sets and with different detectors is presented in figure 4.

The production of electrons from heavy-flavour hadron decays was further studied as a function of the charged-particle pseudorapidity density in pp or p-Pb collisions using the self-normalised yield of heavy-flavour hadron decay electrons. The differential yield measured in a given multiplicity class was divided by its average over all INEL > 0 events ($\text{d}^2N/\text{d}p_{\text{T}}\text{d}\eta / \langle \text{d}^2N/\text{d}p_{\text{T}}\text{d}\eta \rangle_{\text{INEL}>0}$) in pp or p-Pb collisions. All efficiency were obtained as a function of multiplicity. At low p_{T}, the tagging efficiency and the total reconstruction efficiency of electrons from heavy-flavour hadron decays were observed to be multiplicity dependent, while no dependencies were seen at high p_{T}, so the efficiencies cancelled out in the self-normalised ratios at high p_{T}.

5 Systematic uncertainties

The systematic uncertainties on the measured cross sections in pp and p-Pb collisions were obtained separately for the different p_{T} intervals and for the different analyses performed using the TPC-TOF and TPC-EMCal detector combinations. For the self-normalised yield measurements, the systematic uncertainties were estimated directly on the self-normalised yield for each multiplicity class and p_{T} interval. The different sources of systematic uncertainties are discussed in this section and the assigned values are summarised in tables 6, 7, and 8.

The systematic uncertainty on the track reconstruction and selection efficiency was obtained by multiple variations of the track selection criteria, namely, the minimum number of space points in the TPC, the number of TPC crossed rows, the number of TPC $\text{d}E/\text{d}x$ clusters and the number of hits in the ITS.

The uncertainty due to an imperfect description in the simulation of the TPC-TOF (and the TPC-ITS) track matching was estimated by calculating the difference between efficiencies of the TPC-TOF (and the TPC-ITS) track matching in data and MC. To obtain

JHEP08(2023)006

Sources of systematic uncertainties	$0.2 < p_{\mathrm{T}} < 0.5$ GeV/c low-B TPC-TOF	$0.5 < p_{\mathrm{T}} < 4$ GeV/c nominal-B TPC-TOF	$4 < p_{\mathrm{T}} < 35$ GeV/c nominal-B TPC-EMCal
Track selection	negl.	1%	3%
TPC-TOF matching	4%–2%	2%	N/A
TPC-ITS matching	2%	3%	3%
TPC-EMCal matching	N/A	N/A	negl.
SPD hit requirement	25%–15%	10%–3%	5%–negl.
Electron identification	5%	5%–negl.	6%–12%
Hadron contamination	negl.	negl.–2%	negl.–7%
Photonic electron subtraction	20%–11%	7%–1%	negl.
K_{e3} subtraction	15%–1%	N/A	N/A
$\mathrm{W}^{\pm}/\mathrm{Z}^{0} \rightarrow \mathrm{e}$	N/A	N/A	negl.–8%
π^0, η weights	3%–1%	negl.	negl.
RF	N/A	N/A	3%–4%
Luminosity	2.3%	2.3%	2.3%–5%
Total systematic	36%–20%	14%–7%	11%–18%

Table 6. Sources of systematic uncertainties and their assigned values in pp collisions at $\sqrt{s} =$ 13 TeV for $B = 0.2$ T ($0.2 < p_{\mathrm{T}} < 0.5$ GeV/c) and $B = 0.5$ T ($0.5 < p_{\mathrm{T}} < 4$ GeV/c) data sets with the TPC and TOF detectors, as well as with the TPC and EMCal detectors ($4 < p_{\mathrm{T}} < 35$ GeV/c). The values presented as a range correspond to the lowest- and highest-p_{T} intervals.

the matching efficiency, the abundances of primary and secondary particles in data were estimated via template fits to the track impact-parameter distributions, and the relative abundances in the simulation were weighted to match those in data [160, 161]. For the low-B field sample in pp collisions, the uncertainty on the track matching between the ITS and TPC is 2% at $p_{\mathrm{T}} = 0.2$ GeV/c increasing up to 4% at 4 GeV/c, whereas, the uncertainty on the track matching between the TPC and the TOF detector is 4% at $p_{\mathrm{T}} = 0.2$ GeV/c and 2% at 4 GeV/c. In case of the nominal-B field data set, the uncertainty is about 2% for the TPC-TOF track matching and about 3% for the TPC-ITS track matching in the whole p_{T} range. In the p-Pb analysis, the uncertainty for the TPC-TOF track matching, as well as the TPC-ITS track matching, was found to be around 2% in the whole p_{T} range.

The systematic uncertainty on the SPD hit requirement was obtained by varying the condition on the minimum number of hits and the specific layer of the SPD on which a hit was required for both the TPC-TOF and the TPC-EMCal analyses. For the low-B field sample in pp collisions, the systematic uncertainty due to the SPD hit requirement was about 25% at $p_{\mathrm{T}} = 0.2$ GeV/c decreasing to 15% at 0.5 GeV/c, whereas for nominal-B

JHEP08(2023)006

Sources of systematic uncertainties	$0.5 < p_{\mathrm{T}} < 4$ GeV/c nominal-B TPC-TOF	$4 < p_{\mathrm{T}} < 26$ GeV/c nominal-B TPC-EMCal
Track selection	1%	5%–1%
TPC-TOF matching	2%	N/A
TPC-EMCal matching	N/A	negl.
TPC-ITS matching	2%	2%
SPD hit requirement	10%–3%	5%–negl.
Electron identification	3%–1%	1%–5%
Hadron contamination	negl.	negl.–5%
Photonic electron subtraction	7%–1%	negl.
$\mathrm{K_{e3}}$ subtraction	N/A	N/A
$\mathrm{W^{\pm}/Z^0} \rightarrow \mathrm{e}$	N/A	negl.–1%
π^0, η weights	negl.	negl.
RF	N/A	2%–4%
Luminosity	3%	3%
Total systematic	13%–5%	8%–9%

Table 7. Sources of systematic uncertainties and their assigned values in p-Pb collisions at $\sqrt{s_{\mathrm{NN}}} = 8.16$ TeV with TPC and TOF detectors ($0.5 < p_{\mathrm{T}} < 4$ GeV/c), as well as with the TPC and EMCal detectors ($4 < p_{\mathrm{T}} < 26$ GeV/c). The values presented as a range correspond to the lowest- and highest-p_{T} intervals.

field data sets in pp and p-Pb collisions, the uncertainty is about 10% at $p_{\mathrm{T}} = 0.5$ GeV/c decreasing to 5% at 4 GeV/c and becomes negligible in the highest-p_{T} interval.

The uncertainty on the procedure of track matching to EMCal clusters was obtained by varying the $\Delta\eta - \Delta\varphi$ selection using p_{T}-independent thresholds ranging from 0.015 to 0.05 rad in η and φ. The resulting uncertainty was found to be negligible.

The uncertainty on the electron identification originates from imprecisions in the description of the detector response in the MC, as well as from potential biases in the procedure employed to select electron candidates and to estimate the hadron contamination. It was studied by varying the electron identification selection criteria on $n_{\sigma,\mathrm{e}}^{\mathrm{TPC}}$, E/p, and σ^2_{long}. The assigned systematic uncertainties are listed as "Electron identification" in the tables 6, 7, and 8. The assigned systematic uncertainties vary from 5% to 12% depending on the p_{T} and the analysis method.

Additionally, the robustness of the fit procedure used to extract the hadron contamination in both electron identification strategies was checked. In the TPC-TOF analysis,

JHEP08(2023)006

different analytical functions were utilised to parameterise the TPC $\mathrm{d}E/\mathrm{d}x$, which had negligible effects on the estimated hadron contamination up to a p_{T} of 3 GeV/c. In the TPC-EMCal analysis, the scaling region of the hadron E/p distribution was varied. The resulting uncertainties were found to be negligible at low p_{T} and of the order of 5% at high p_{T}.

The uncertainty on the subtraction of photonic electrons is related to the efficiency of finding the partner electron and was studied by varying the selection of partner tracks, i.e. the number of TPC clusters used for $(\mathrm{d}E/\mathrm{d}x)$ calculation and the minimum p_{T} requirement, as well as the selection on the invariant mass of $\mathrm{e}^{+}\mathrm{e}^{-}$ pairs.

The subtraction of K_{e3} decay electrons in pp collisions for $p_{\mathrm{T}} < 0.5\,\mathrm{GeV}/c$ can be affected by the uncertainty on the parameterisation of the ratio of K_{e3} to photonic electrons, and was found to result in an uncertainty of 15% at $p_{\mathrm{T}} = 0.2$ GeV/c and to be negligible at $p_{\mathrm{T}} \geq 0.5\,\mathrm{GeV}/c$.

The uncertainty on the contribution of electrons from $\mathrm{W}^{\pm}$ and Z^{0} boson decays was estimated by varying the yield of electrons from $\mathrm{W}^{\pm}$ and Z^{0} boson decays by 25%. The strategy is imported from the most recent measurements from ALICE [16, 141]. The resulting uncertainty was found to be negligible for p-Pb collisions and only relevant at very high p_{T} for pp collisions, where it amounts to about 8%.

In the MC simulations, the π^{0} and η meson p_{T} distributions were weighted such that their measured p_{T} spectra are reproduced. The uncertainty from the measurements was propagated to the efficiency of finding the partner electron by parameterising the data along the upper and lower ends of their statistical and systematic uncertainties added in quadrature. The uncertainty was found to be about 3% at $p_{\mathrm{T}} = 0.2$ GeV/c in pp collisions and to be negligible at $p_{\mathrm{T}} \geq 0.5\,\mathrm{GeV}/c$ in both pp and p-Pb collisions.

The systematic uncertainty on the trigger RF, as explained in section 4.3, was propagated on the p_{T}-differential cross section of electrons from heavy-flavour hadron decays. The uncertainty was of the order of 4% at the highest p_{T}.

The systematic uncertainty on the luminosity was propagated on the p_{T}-differential cross section of electrons from heavy-flavour hadron decays. The uncertainty was 2.3% to 5% in pp collisions depending on the p_{T}, as the uncertainty from the rejection factors for triggered samples were taken into consideration, and 3% in p-Pb collisions, where the uncertainty from the rejection factors contributed negligibly to the uncertainty on luminosity.

As the geometrical acceptance and reconstruction efficiencies are essentially independent of $\mathrm{d}N_{\mathrm{ch}}/\mathrm{d}\eta$ in the measured multiplicity range, these corrections and their corresponding systematic uncertainties largely cancel in the ratio to the multiplicity-integrated yield, thus resulting in a lower systematic uncertainty for self-normalised yields compared to the one for the p_{T} spectra.

The total systematic uncertainties on the p_{T} spectra and the self-normalised yields were calculated by summing the different contributions in quadrature, as they are considered to be uncorrelated.

JHEP08(2023)006

		pp, $\sqrt{s} = 13$ TeV			p-Pb, $\sqrt{s_{NN}} = 8.16$ TeV		
	Multiplicity	p_T interval (GeV/c)			p_T interval (GeV/c)		
	intervals	0.5–6	6–12	15–30	0.5–6	6–8	14–26
Track selection	I	negl.	2%	2%	negl.	3%	3%
	III	negl.	2%	2%	negl.	3%	3%
	V	negl.	2%	2%	negl.	4%	4%
SPD hit requirement	I	10%	6%	14%	10%	2%	10%
	III	3%	6%	6%	2%	2%	2%
	V	4%	6%	6%	2%	2%	2%
Electron identification	I	1%	3%	3%	1%	2%	2%
	III	1%	3%	3%	1%	2%	2%
	V	1%	3%	3%	1%	4%	4%
Photonic electron subtraction	I	1%	1%	2%	1%	1%	1%
	III	1%	2%	2%	1%	1%	1%
	V	1%	2%	2%	1%	1%	1%
Total systematics	I	10%	7%	15%	10%	4%	11%
	III	3%	7%	7%	2%	4%	4%
	V	4%	7%	7%	2%	6%	6%

Table 8. Systematic uncertainty on self-normalised yield in pp collisions at $\sqrt{s} = 13$ TeV and p-Pb collisions at $\sqrt{s_{NN}} = 8.16$ TeV.

6 Results

6.1 p_T-differential cross section of heavy-flavour hadron decay electrons in pp and p-Pb collisions

The p_T-differential production cross section of electrons from semileptonic decays of heavy-flavour hadrons at midrapidity in pp collisions at $\sqrt{s} = 13$ TeV measured in the transverse momentum interval $0.2 < p_T < 35$ GeV/c is shown in figure 5. The statistical uncertainties are represented as vertical lines while the total systematic uncertainties are

JHEP08(2023)006

displayed as boxes. In the top left panel of figure 5, the cross sections measured with the TPC-TOF detectors and the two different data sets collected with different magnetic fields are plotted together with the spectra obtained using the TPC-EMCal detectors with MB triggered events, as well as with EMCal triggered events, EG1, and EG2. The ratios of the different analyses in the overlapping p_{T} intervals are shown in the bottom left panel of figure 5. For $0.5 < p_{\mathrm{T}} < 4$ GeV/c, the ratio of the result from the TPC-TOF analyses with $B = 0.5$ T to the one obtained with $B = 0.2$ T is displayed. In $3 < p_{\mathrm{T}} < 4$ GeV/c, the ratio of the cross section obtained from the TPC-TOF analysis to that obtained from the TPC-EMCal analysis is shown for MB triggered events. At higher p_{T}, namely $6 < p_{\mathrm{T}} < 10$ GeV/c ($12 < p_{\mathrm{T}} < 18$ GeV/c), the ratio of the TPC-EMCal results for MB and EG2 (EG2 and EG1) triggered events is reported. All ratios are consistent with unity within statistical and systematic uncertainties, which demonstrates that the different analyses are in agreement with each other. The final cross section in the p_{T} intervals 0.2–0.5 GeV/c, 0.5–4 GeV/c, 4–6 GeV/c, 6–12 GeV/c, and 12–35 GeV/c was obtained from the TPC-TOF low-B field analysis, the TPC-TOF nominal-B field analysis, and from the results obtained with the TPC-EMCal detectors using MB, EG2 and EG1 triggered events, respectively. In this way, for each p_{T} range, the measurement with the smallest total uncertainty (quadratic sum of statistical and systematic uncertainty) is used.

The p_{T}-differential cross section measurement was compared with FONLL [34] and GM-VFNS [32] pQCD calculations,[1] as shown in the right panel of figure 5. The uncertainties of the FONLL calculations reflect different choices for the charm- and beauty-quark masses, and for the factorisation and renormalisation scales as well as the uncertainty on the set of parton distribution functions (PDF) (CTEQ6.6 [162]). The FONLL calculations describe the measurements within the uncertainties, although the theoretical uncertainties are large, up to a factor of two. The data are found to be close to the upper edge of the FONLL prediction, which can be clearly seen in the right bottom panel of figure 5, where the ratio of the data points to the FONLL calculations is shown. Similar observations were made for the measurements of electrons from heavy-flavour hadron decays in pp collisions at lower energies at the LHC [9, 142, 153, 154] and at RHIC [163, 164]. The measurement of the cross section of D mesons is also consistent with upper bound of FONLL pQCD calculations in pp collisions at LHC [5, 6, 8, 12, 13, 160, 165] and RHIC [166], as well as in $\mathrm{p\bar{p}}$ collisions at Tevatron energies [167]. The FONLL calculations use fragmentation functions tuned on $\mathrm{e^+e^-}$ data and assume that all charm quarks fragment only into $\mathrm{D^+}$ and $\mathrm{D^0}$ mesons (and their antiparticles). Recent measurements of charm-baryon production at midrapidity in pp and p-Pb collisions from ALICE show a baryon-to-meson ratio significantly higher than that in $\mathrm{e^+e^-}$ collisions, suggesting that the fragmentation of charm quark is not universal across different collision systems [14, 168]. As a consequence, calculations taking properly into account the latest open-cham baryon measurements at midrapidity to constrain the charm fragmentation are expected to predict a smaller yield of

[1] Central values : FONLL : $\mu_{\mathrm{F}} = \mu_{\mathrm{R}} = \sqrt{m_{\mathrm{Q}}^2 + p_{\mathrm{T}}^2}$, $m_{\mathrm{b}} = 4.75$ GeV, $m_{\mathrm{c}} = 1.5$ GeV; GM − VFNS : $\mu_{\mathrm{F}} = 0.49\ \mu_{\mathrm{R}}, \mu_{\mathrm{R}} = \sqrt{4m_{\mathrm{Q}}^2 + p_{\mathrm{T}}^2}$, $m_{\mathrm{b}} = 4.5$ GeV, $m_{\mathrm{c}} = 1.5$ GeV; where μ_{R} = renormalization scale, μ_{F} = factorisation scale.

JHEP08(2023)006

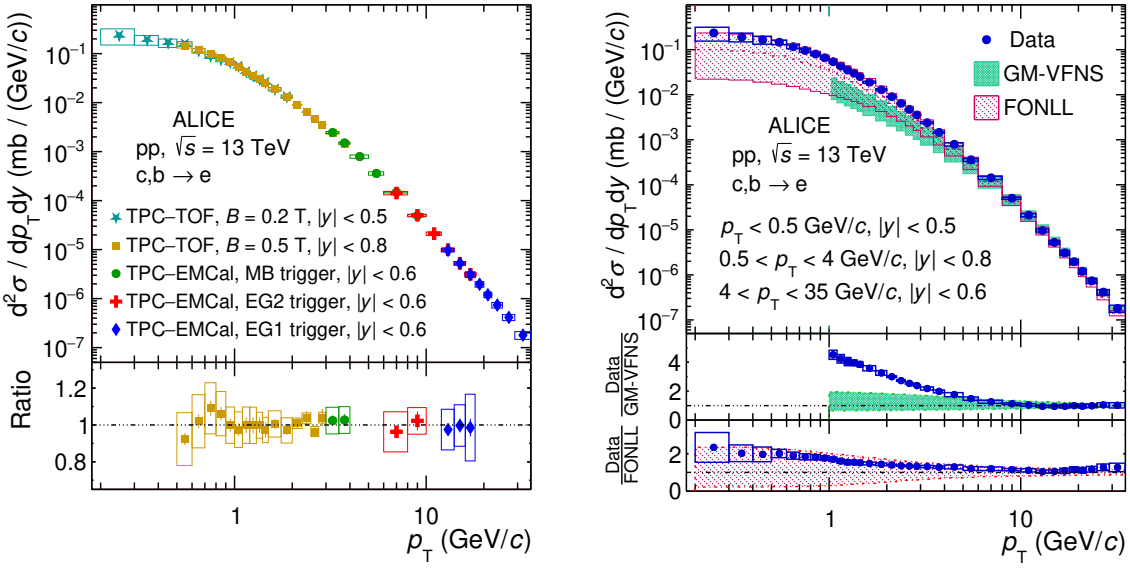

Figure 5. Left, top: p_{T}-differential cross section of electrons from heavy-flavour hadron decays in pp collisions at $\sqrt{s} = 13$ TeV measured at midrapidity with different detectors and data sets. Left, bottom: ratios of the different measurements in the overlapping p_{T} intervals. Right: p_{T}-differential cross section compared with Fixed Order with Next-to-Leading-Log resummation (FONLL) [34] and General-mass-variable-flavour-number-Scheme (GM-VFNS) [33] predictions and its ratios with respect to FONLL and GM-VFNS central values in the two lower panels. Vertical bars and boxes denote statistical and systematical uncertainties, respectively.

heavy-flavour hadron decays by about 9% compared to the FONLL spectrum. The largest source of uncertainties in the GM-VFNS prediction is due to scale variation, and hence PDF related uncertainties and variations of the bottom and charm mass are not considered. The GM-VFNS framework includes leptoproduction from the following three steps: beauty quark to beauty hadrons (b → B), transition from beauty quark to charm hadrons (b → B → D), and charm quark to charm hadrons (c → D). The GM-VFNS calculations describe the data within the uncertainties for p_{T} greater than 5 GeV/c, but largely underestimate the cross section for lower p_{T}, up to a factor of five at 1 GeV/c, as seen in the right middle panel of figure 5. Similar observations were reported for the non-prompt D meson measurements at $\sqrt{s} = 5.02$ TeV [165]. For prompt D mesons at $\sqrt{s} = 5.02$ TeV, however, the GM-VFNS predictions describe the cross section within the uncertainties [165]. Electrons from heavy-flavour hadron decays are dominated by semileptonic decays of beauty hadrons for $p_{\mathrm{T}} > 5$ GeV/c [28, 169]. Therefore, the cross section measured up to 35 GeV/c can provide important information to beauty hadron production.

The p_{T}-differential production cross section of electrons from semileptonic heavy-flavour hadron decays at midrapidity in p-Pb collisions at $\sqrt{s_{\mathrm{NN}}} = 8.16$ TeV measured in the transverse momentum interval $0.5 < p_{\mathrm{T}} < 26$ GeV/c is shown in figure 6. In the upper panel of figure 6, the cross sections measured with the TPC-TOF detectors are plotted together with the measurements obtained using the TPC-EMCal detectors with MB and EMCal EG2 and EG1 triggered events. On the bottom left panel of figure 6, the

JHEP08(2023)006

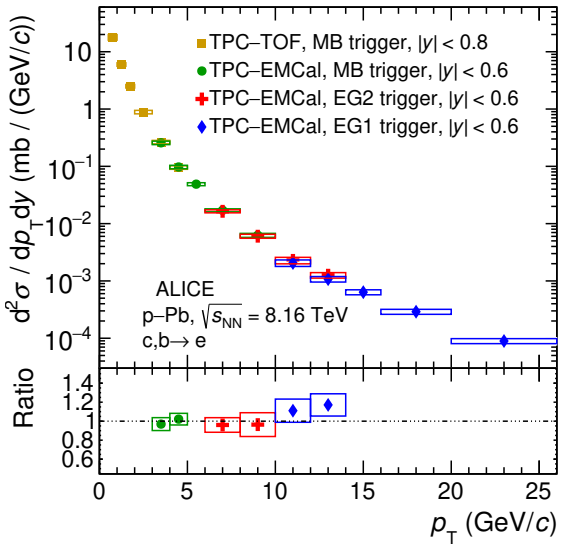

Figure 6. Top: p_{T}-differential cross section of electrons from heavy-flavour hadron decays in p-Pb collisions at $\sqrt{s_{\mathrm{NN}}} = 8.16$ TeV measured at midrapidity with different detectors. Bottom: ratios of the different measurements in the overlapping p_{T} intervals.

ratios of the cross sections obtained from the different measurements are calculated in the overlapping p_{T} intervals. For $3 < p_{\mathrm{T}} < 5$ GeV/c, the ratio of the result obtained from the TPC-TOF analysis with respect to that from the TPC-EMCal is shown for MB triggered events. For $6 < p_{\mathrm{T}} < 10$ GeV/c ($12 < p_{\mathrm{T}} < 14$ GeV/c) the ratio of the TPC-EMCal results obtained with MB and EG2 triggered events (EG2 and EG1) is reported. All ratios are consistent with unity within statistical and systematic uncertainties. The same strategy as in pp collisions was used to get the final cross section in p-Pb collisions. The final cross section in the p_{T} intervals 0.5–4 GeV/c, 4–6 GeV/c, 6–9 GeV/c, and 9–26 GeV/c was obtained from the TPC-TOF nominal-B field analysis and from the results using the TPC-EMCal detectors with MB, EG2, and EG1 triggered events, respectively.

6.2 Nuclear modification factor of electrons from heavy-flavour hadron decays in p-Pb collisions

The nuclear modification factor of electrons from heavy-flavour hadron decays, R_{pPb}, is defined as

$$R_{\mathrm{pPb}}(p_{\mathrm{T}}, y) = \frac{1}{A} \frac{\mathrm{d}^2\sigma_{\mathrm{pPb}}/\mathrm{d}p_{\mathrm{T}}\mathrm{d}y}{\mathrm{d}^2\sigma_{\mathrm{pp}}/\mathrm{d}p_{\mathrm{T}}\mathrm{d}y}, \tag{6.1}$$

where $\mathrm{d}^2\sigma_{\mathrm{pPb}}/\mathrm{d}p_{\mathrm{T}}\mathrm{d}y$ is the cross section of electrons from heavy-flavour hadron decays measured in p-Pb collisions at $\sqrt{s_{\mathrm{NN}}} = 8.16$ TeV and $\mathrm{d}^2\sigma_{\mathrm{pp}}/\mathrm{d}p_{\mathrm{T}}\mathrm{d}y$ is the cross section of electrons from heavy-flavour hadron decays in pp collisions at the same centre-of-mass energy, scaled with the number of nucleons (A) in the lead ion. The reference cross section in pp collisions was obtained using the measurement at $\sqrt{s} = 13$ TeV, presented here. The cross section at $\sqrt{s} = 13$ TeV was scaled to $\sqrt{s} = 8.16$ TeV using pQCD calculations. The p_{T}-dependent scaling factor was obtained by calculating the ratio of the production cross

JHEP08(2023)006

sections of electrons from heavy-flavour hadron decays from FONLL calculations [34] at $\sqrt{s} = 8.16\,\text{TeV}$ to $\sqrt{s} = 13\,\text{TeV}$. The systematic uncertainty on the pp reference includes the systematic uncertainties on the measured cross section at $\sqrt{s} = 13\,\text{TeV}$, which was described above, and the ones on the p_{T}-dependent scaling factor. The uncertainty on the scaling factor ranges between 11% and 1% going from $p_{\text{T}} = 0.2$ GeV/c to $p_{\text{T}} = 26$ GeV/c. This includes the uncertainties on the PDFs, quark masses, and factorisation and renormalisation scales, as described in ref. 170. The two contributions were added in quadrature leading to a total systematic uncertainty of 5-15%, depending on p_{T}. In addition, a global normalisation systematic uncertainty of 2.3% from the pp analysis at $\sqrt{s} = 13\,\text{TeV}$ was also considered. The p_{T}-differential cross section of electrons from heavy-flavour hadron decays in pp collisions at $\sqrt{s} = 13$ TeV scaled to $\sqrt{s} = 8.16$ TeV using the aforementioned procedure is shown together with the p_{T}-differential cross section of electrons from heavy-flavour hadron decays in p-Pb collisions at $\sqrt{s_{\text{NN}}} = 8.16$ TeV in figure 7.

The nuclear modification factor of electrons from heavy-flavour hadron decays as a function of transverse momentum at $\sqrt{s_{\text{NN}}} = 8.16\,\text{TeV}$ is presented in figure 8. The statistical and systematic uncertainties of the spectra in p-Pb and pp collisions were propagated as uncorrelated. The normalisation uncertainties are shown as a solid box at $R_{\text{pPb}} = 1$. The R_{pPb} is consistent with unity within statistical and systematic uncertainties over the whole p_{T} range of the measurement. Modifications of the cross section of electrons from heavy-flavour hadron decays in p-Pb collisions due to different cold nuclear matter effects, are small compared to the current uncertainties of the measurement in the probed p_{T} range. The sample of electrons from heavy-flavour hadron decays is dominated by beauty-hadron decays for $p_{\text{T}} > 5\,\text{GeV}/c$ [28, 171]. The R_{pPb} was fitted with a constant function above 5 GeV/c and the value was $0.95 \pm 0.02(\text{stat.}) \pm 0.13(\text{sys.})$, thus consistent with unity within 13%. The R_{pPb} of unity indicates that the beauty production is not modified in p-Pb collisions within the kinematic range of this measurement, which is also consistent with the measurement of R_{pPb} of beauty-decay electrons up to $p_{\text{T}} = 8\,\text{GeV}/c$ at $\sqrt{s_{\text{NN}}} = 5.02\,\text{TeV}$ [19]. In the right panel of figure 8, the R_{pPb} at $\sqrt{s_{\text{NN}}} = 8.16\,\text{TeV}$ is compared with that at $\sqrt{s_{\text{NN}}} = 5.02\,\text{TeV}$ and different theoretical models provided for $\sqrt{s_{\text{NN}}} = 5.02\,\text{TeV}$ [141]. The R_{pPb} is observed to be independent of the centre-of-mass energy. The data disfavour the enhancement trend at low p_{T} predicted by the model calculations which are based on incoherent multiple scatterings [172]. Model predictions which are based on coherent multiple scattering and energy loss in the CNM, pQCD calculations using FONLL framework and EPS09NLO for the nuclear modification of the PDF, as well as calculations which assume the formation of a hydrodynamical expanding medium in p-Pb collisions at $\sqrt{s_{\text{NN}}} = 5.02\,\text{TeV}$ within the Blast wave framework predict an R_{pPb} close to unity and are in agreement with the measurements.

6.3 Self-normalised yield of electrons from heavy-flavour hadron decays vs. normalised multiplicity in pp and p-Pb collisions

The self-normalised yield of electrons from heavy-flavour hadron decays as a function of the self-normalised charged-particle pseudorapidity density at midrapidity, i.e., $\mathrm{d}^2N/\mathrm{d}p_{\text{T}}\mathrm{d}y/\langle \mathrm{d}^2N/\mathrm{d}p_{\text{T}}\mathrm{d}y\rangle_{\text{INEL}>0}$ vs. $\mathrm{d}N_{\text{ch}}/\mathrm{d}\eta/\langle \mathrm{d}N_{\text{ch}}/\mathrm{d}\eta\rangle$, in pp collisions at $\sqrt{s} = 13\,\text{TeV}$

JHEP08(2023)006

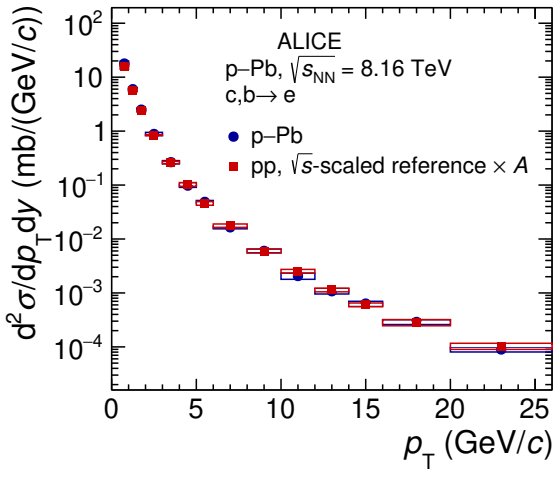

Figure 7. p_{T}-differential cross section of electrons from heavy-flavour hadron decays measured in p-Pb collisions at $\sqrt{s_{\mathrm{NN}}} = 8.16$ TeV compared with the pp reference at the same centre-of-mass energy obtained from the measurement in pp collisions at $\sqrt{s} = 13$ TeV scaled to $\sqrt{s} = 8.16$ TeV.

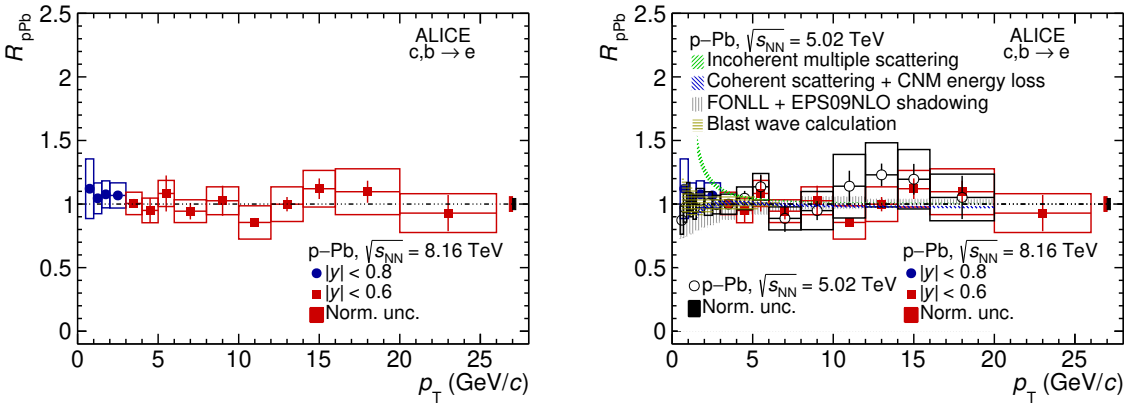

Figure 8. The nuclear modification factor R_{pPb} of electrons from heavy-flavour hadron decays in p-Pb collisions at $\sqrt{s_{\mathrm{NN}}} = 8.16$ TeV (left) compared with that at $\sqrt{s_{\mathrm{NN}}} = 5.02$ TeV and theoretical models at $\sqrt{s_{\mathrm{NN}}} = 5.02$ TeV (right) [141].

is presented in figure 9. The results are self-normalised to the INEL > 0 event class. The measurements were performed in five p_{T} intervals from 0.5 to 30 GeV/c. The dashed line shown in the figure is a linear function with a slope of unity. The available data samples allow us to examine events with a multiplicity more than six times larger than the average multiplicity in pp collisions. The self-normalised yield of electrons from heavy-flavour hadron decays grows faster than linear with the self-normalised multiplicity. The measurement in intervals of p_{T} shows that this increase is more pronounced for high-p_{T} electrons. The yield of heavy-flavour decay electrons increases by approximately a factor of nine with respect to its multiplicity-integrated value for the lowest measured p_{T} interval ($0.5 < p_{\mathrm{T}} < 1.5$ GeV/c) and a factor of 29 for the highest measured p_{T} interval ($20 < p_{\mathrm{T}} < 35$ GeV/c) for multiplicities of six times the average multiplicity.

JHEP08(2023)006

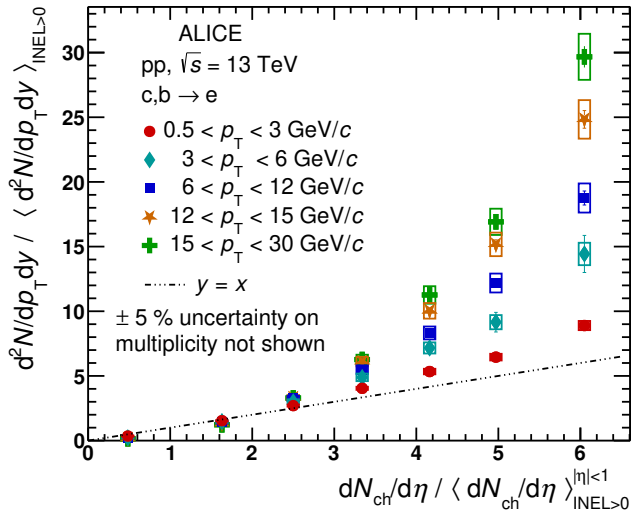

Figure 9. Self-normalised yield of electrons from heavy-flavour hadron decays as a function of normalised charged-particle pseudorapidity density at midrapidity computed in pp collisions at $\sqrt{s}$ = 13 TeV in different p_T intervals.

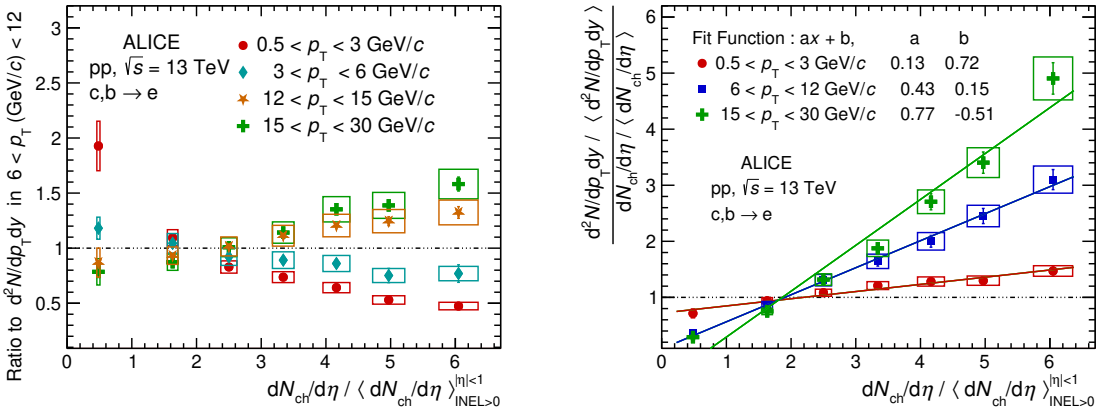

Figure 10. Ratio of the self-normalised yields in different p_T intervals with respect to that in the $6 < p_T < 12$ GeV/c interval (left) and double ratio of the self-normalised yields of electrons to the self-normalised multiplicity (right) in pp collisions at $\sqrt{s} = 13$ TeV for three p_T ranges.

In the left panel of figure 10, the ratios of the self-normalised yields of electrons from heavy-flavour hadron decays in various p_T intervals with respect to the one measured in the $6 < p_T < 12$ GeV/c interval are shown. The yield of lower-p_T electrons is higher in low multiplicity events, while it decreases in higher multiplicity events. An opposite trend is observed for electrons at higher p_T, where the yield is lower in low multiplicity events and increases at higher multiplicities. The increase of the slope with p_T is influenced by the momentum dependence of jet fragmentation affecting the measured multiplicity at midrapidity, and the momentum dependence of the fraction of electrons from charm and beauty hadron decays. The relative fraction of electrons from beauty hadron decays

JHEP08(2023)006

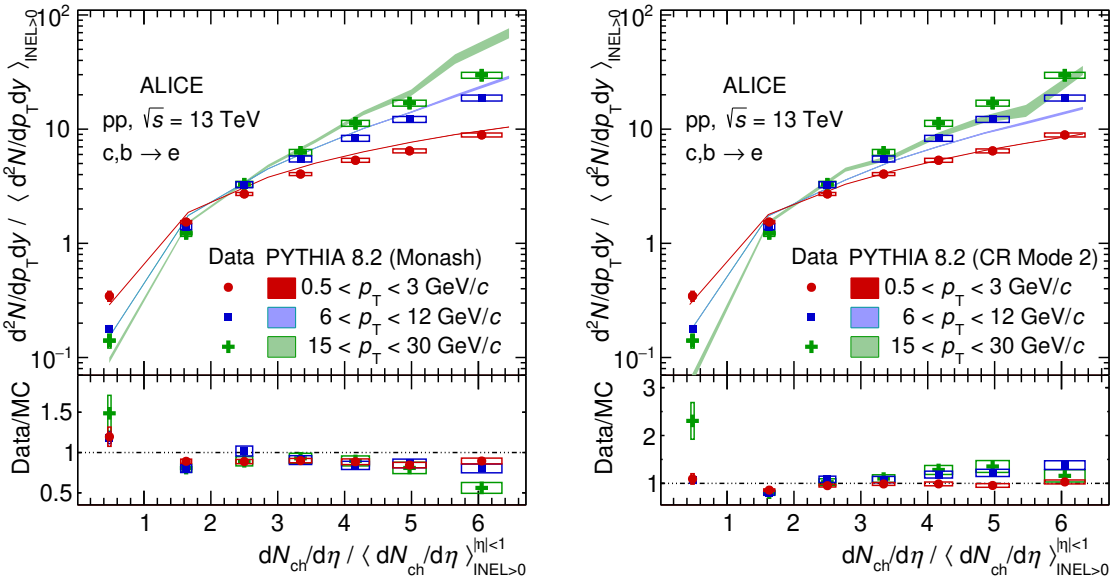

Figure 11. Comparison of the self-normalised yield of electrons from heavy-flavour hadron decays as a function of multiplicity measured in pp collisions at $\sqrt{s} = 13$ TeV for different p_T intervals with PYTHIA 8.2 Monash tune (left) and PYTHIA 8.2 with CR mode 2 (right). The width of the band is the statistical uncertainty from PYTHIA simulations. The bottom panel shows the ratio of data with respect to the MC predictions. The vertical bars correspond to the propagated statistical error from the data and the MC predictions, and the boxes correspond to systematical uncertainties from the data.

increases with p_T and becomes the main source of heavy-flavour hadron decay electrons at high p_T ($p_T > 5\,\text{GeV}/c$) [106, 107, 173].

In the right panel of figure 10, the double ratio of the self-normalised electron yield to the self-normalised multiplicity in pp collisions is presented. The double ratio is observed to increase with multiplicity. The increase is weaker for low-p_T electrons than for high-p_T electrons. A linear function was used to fit the multiplicity dependence of the double ratio, which was found to describe the data reasonably well for all p_T intervals. This indicates that in the measured p_T range the yield grows approximately with the square of the multiplicity with a slope increasing with p_T.

The self-normalised yield of electrons from heavy-flavour hadron decays is compared in figure 11 with PYTHIA 8.2 simulations using different tunes. In the PYTHIA 8.2 framework, multiparton interactions (MPI) and the colour reconnection (CR) mechanism are implemented, which reproduce the charged-particle multiplicity distribution measured at the LHC [111, 174]. These mechanisms are important in order to describe the stronger than linear increase of charm and beauty production with multiplicity as demonstrated in [106]. The charged-particle multiplicity also includes particles directly produced in the same hard partonic scattering process in which the heavy quark is created, making them strongly related. These dependencies come from the initial- and final-state radiations, decays of heavy-flavour hadrons, and charged particles produced in the jet fragmentation and are known

JHEP08(2023)006

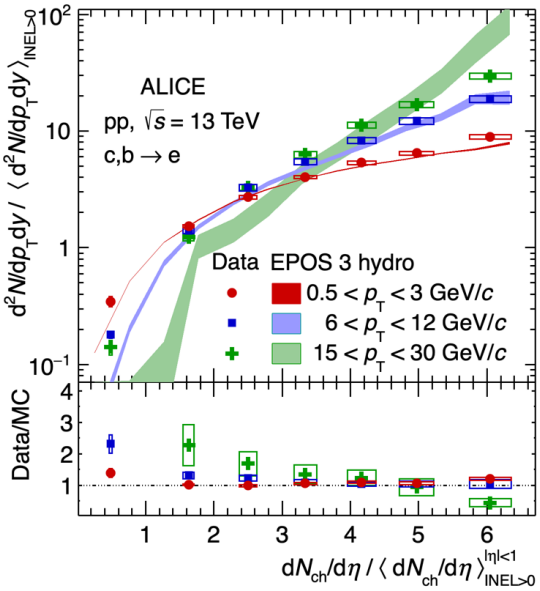

Figure 12. Comparison of self-normalised yield of electrons from heavy-flavour hadron decays as a function of multiplicity measured in pp collisions at $\sqrt{s} = 13$ TeV for different p_T intervals with EPOS 3 hydro calculations. The width of the band is the statistical uncertainty from EPOS simulations. The bottom panel shows the ratio of data with respect to the MC predictions. The vertical bars correspond to the propagated statistical error from the data and the MC predictions, and the boxes correspond to systematical uncertainties from the data. The ratio for the lowest multiplicity point for $15 < p_T < 30$ GeV/c (not shown in the figure) is 13±18.

as auto-correlation effects. A study of the self-normalised yield of heavy-flavour particles using the PYTHIA 8.2 generator shows that the stronger than linear increase of the yield of heavy-flavour particles is mainly driven by auto-correlation effects. In the absence of auto-correlation effects the increase of the yield of particles produced in hard scattering processes is weaker than linear for multiplicities exceeding about three times the mean multiplicity [173]. In PYTHIA 8.2, the p_T dependence of the increase of the self-normalised yield with multiplicity is also due to auto-correlation effects introduced by the parton fragmentation because high momentum partons are accompanied by a larger number of fragments which contribute to the multiplicity. In the case of electrons from heavy-flavour hadron decays, the high-p_T part of the spectra is dominated by beauty decay electrons, whose yield was demonstrated to have a more pronounced increase with multiplicity due to the larger jet activity [173]. In the left panel of figure 11, the measured self-normalised yield of electrons from heavy-flavour hadron decays is compared to calculations with the PYTHIA 8.2 Monash tune that describe the overall trend in data, but the slope is overestimated at high p_T. In the right panel of figure 11, an improved tune which includes string formation beyond the leading-colour approximation i.e. PYTHIA 8.2 with CR mode 2 [101, 175], is shown to reproduce the p_T dependence, however the slope is underestimated at high p_T.

Calculations with the EPOS 3 event generator [117] are able to reproduce the data well, except for the highest measured p_T interval, as can be seen in figure 12. In the

JHEP08(2023)006

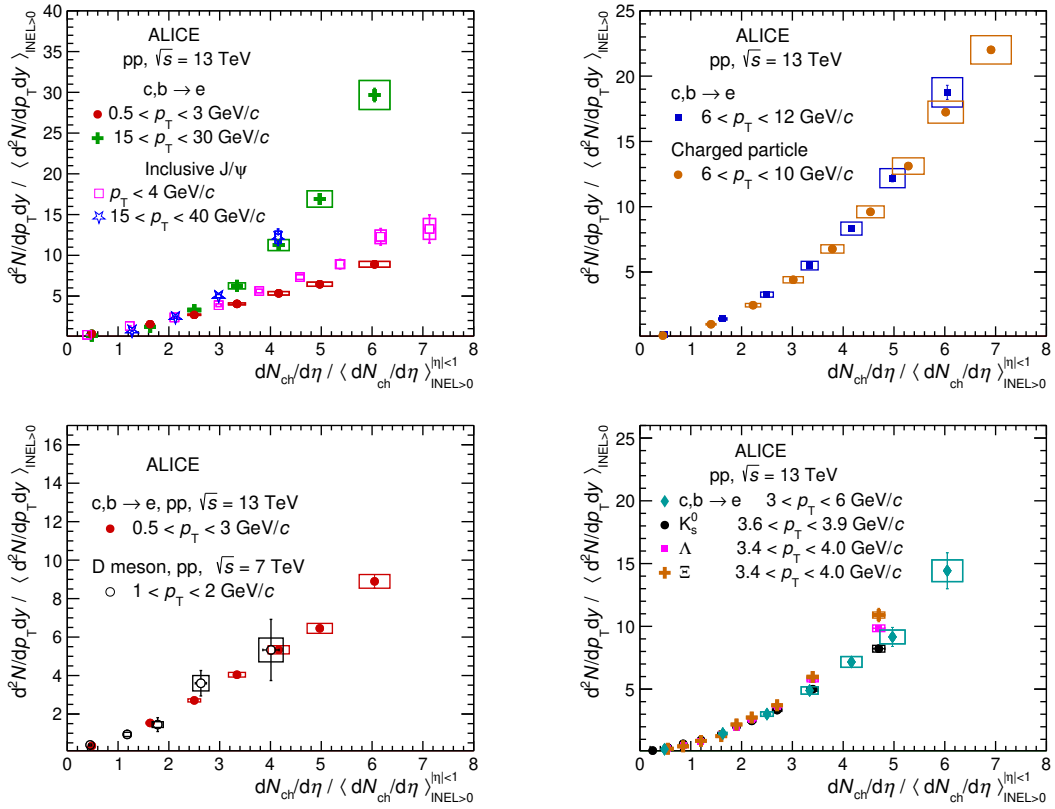

Figure 13. Comparison of the self-normalised yield of electrons from heavy-flavour hadron decays measured in pp collisions at $\sqrt{s} = 13$ TeV with the self-normalised yields of J/ψ in pp collisions at $\sqrt{s} = 13$ TeV (top left), charged particles in pp collisions at $\sqrt{s} = 13$ TeV (top right), D mesons in pp collisions at $\sqrt{s} = 7$ TeV (bottom left) and strange particles in pp collisions at $\sqrt{s} = 13$ TeV (bottom right), in comparable p_{T} bins.

EPOS 3 model, the elementary scattering objects are pomerons, which are exchanged between the partons participating in the collision. The pomerons consist of a hard pQCD scattering vertex, accompanied by initial (space-like) and final (time-like) state parton emission. The production of a hard probe is more likely from events with hard pomeron exchanges. This implies that for a given charged-particle multiplicity the presence of heavy-flavour hadrons favours events with fewer but harder pomerons, which leads to a stronger than linear increase of heavy-flavour production with charged-particle multiplicity. The increase also gets stronger with the increasing p_{T}, which, as discussed above for the case of PYTHIA 8.2 simulations, is related to the hardness of the partonic scattering and the accompanying jet activity in the event. The subsequent hydrodynamic evolution of the system then amplifies the increase because the charged-particle multiplicity is reduced by the hydrodynamic expansion, in contrast to the heavy-flavour production. The charged-particle multiplicity is reduced because part of the available energy goes into flow rather than particle production [176].

JHEP08(2023)006

The trend of the self-normalised yield of electrons in pp collisions as a function of self-normalised multiplicity is compared in figure 13 with the self-normalised yield of other particles measured by the ALICE Collaboration, namely J/ψ [107], charged particles [114], strange hadrons [177] in pp collisions at $\sqrt{s}$ = 13 TeV, and D mesons [106] in pp collisions at $\sqrt{s}$ = 7 TeV. The self-normalised yields for strange hadrons were calculated using the multiplicity-dependent cross section measurements reported in [177]. These self-normalised yields allow a direct comparison of multiplicity-dependent production of different particle species, with the advantage that the charged-particle pseudorapidity density is measured using the same detector and procedure. The p_{T} ranges of electrons are selected to be similar to the measured p_{T} range of the compared particles, with a caveat that the p_{T} interval of electron parents (heavy-flavour hadrons) is considerably broader and shifted towards higher p_{T} values compared to the one of the electrons. The slope of the increase of the self-normalised yield of electrons from heavy-flavour hadron decays as a function of self-normalised multiplicity at midrapidity is similar to that measured for J/ψ, charged particles, strange mesons, and D mesons in similar p_{T} ranges. At high and intermediate p_{T}, the production of hadrons is dominated by hard partonic scattering processes, independent of the particle species, accompanied by jet activity in the event. For heavy-flavour particles this is also true at low p_{T} due to the large charm and beauty quark masses. As it was discussed above, in PYTHIA 8.2, the particle production associated with jet activity leads to strong auto-correlation effects, which give rise to the observed stronger than linear increase of particle yields, making the self-normalised yield of the different particles reported here compatible with each other.

The self-normalised yield of electrons from heavy-flavour hadron decays as a function of the self-normalised charged-particle pseudorapidity density for p-Pb collisions at $\sqrt{s_{\mathrm{NN}}}$ = 8.16 TeV is presented in figure 14. The results are self-normalised to the INEL$>$ 0 event class, similarly to pp collisions. The dashed line is a linear function with a slope of unity as shown in the figure. The measurements were performed in five p_{T} intervals from 0.5 GeV/c to 26 GeV/c. Events with multiplicity more than four times larger than the average multiplicity in p-Pb collisions are studied. The self-normalised yield of electrons from heavy-flavour hadron decays grows faster than linear with the self-normalised multiplicity. The measurements in p_{T} intervals show no p_{T} dependence within the uncertainties of the measurement. The yield increase is approximately a factor of seven for multiplicities four times larger than the average multiplicity.

In the left panel of figure 15, the ratios of the self-normalised yield of electrons from heavy-flavour hadron decays in various p_{T} intervals with respect to the one measured in the $3 < p_{\mathrm{T}} < 6$ GeV/c interval are shown. Contrary to the pp collision case, within the uncertainties no p_{T} dependence is observed. The right panel of figure 15 shows the double ratio of the self-normalised heavy-flavour hadron decay electron yield to the self-normalised multiplicity. The double ratio increases with multiplicity, with no dependence on p_{T}. The double ratio was fitted with a linear function, which reasonably describes the data for all p_{T} intervals. This indicates that in the measured p_{T} range the yield increases approximately with the square of the multiplicity with a similar coefficient for all p_{T} intervals.

JHEP08(2023)006

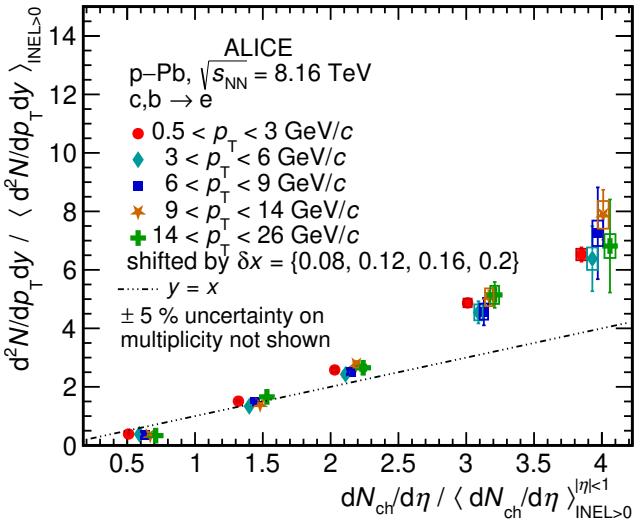

Figure 14. Self-normalised yield of electrons from heavy-flavour hadron decays as a function of self-normalised charged-particle pseudorapidity density at midrapidity measured in p-Pb collisions at $\sqrt{s_{NN}} = 8.16$ TeV in different p_T intervals. The position of the points on the x-axis are shifted horizontally by δx to improve the visibility.

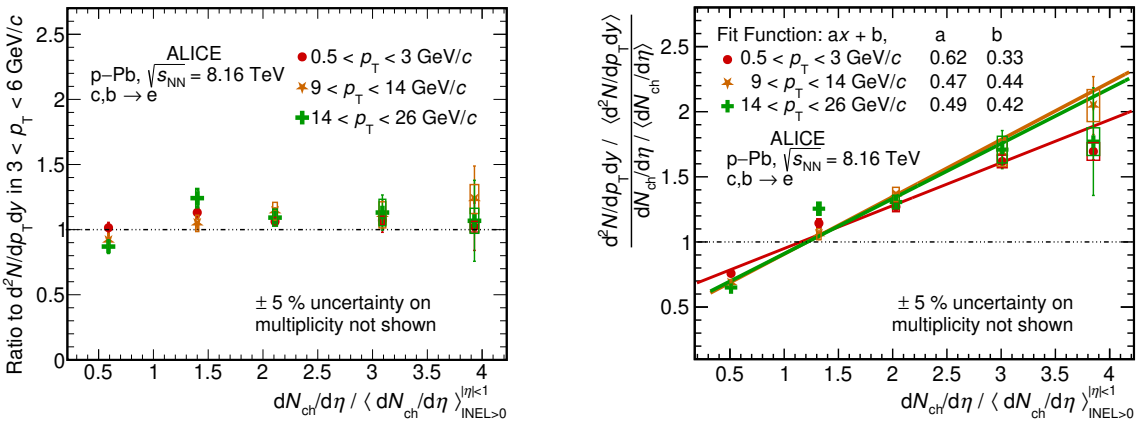

Figure 15. Ratio of the self-normalised yield in different p_T intervals with respect to that in the $3 < p_T < 6$ GeV/c interval (left). Double ratio of the self-normalised yield of heavy-flavour hadron decay electrons to the self-normalised multiplicity in p-Pb collisions at $\sqrt{s_{NN}} = 8.16$ TeV in three p_T ranges (right).

Though the self-normalised yields of electrons from heavy-flavour hadron decays in pp and p-Pb collisions show similar features in their increase with multiplicity, a quantitative comparison of the measurements between the two systems is not straightforward. In pp collisions, a high multiplicity event arises mostly from hard events, with multiparton interactions and jets fragmenting in multiple hadrons. In p-Pb collisions, the multiplicity dependence of heavy-flavour production is also driven by the presence of multiple binary nucleon-nucleon interactions, which make the contribution from possible auto-correlation

JHEP08(2023)006

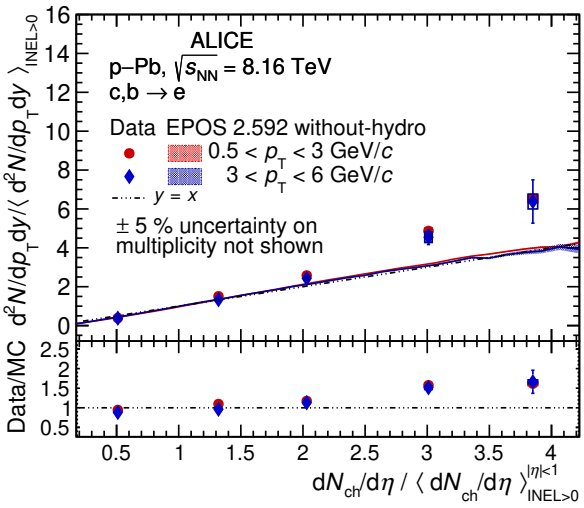

Figure 16. Self-normalised yields of electrons from heavy-flavour hadron decays as a function of self-normalised charged-particle pseudorapidity density at midrapidity measured in p-Pb collisions at $\sqrt{s_{NN}}$ = 8.16 TeV compared with EPOS 2.592 without-hydrodynamics in two p_T intervals 0.5 < p_T < 3 GeV/c and 3 < p_T < 6 GeV/c. The width of the band is the statistical uncertainty from EPOS simulations. The bottom panel shows the ratio of data with respect to the MC predictions. The vertical bars correspond to the propagated statistical uncertainties from the data and the MC predictions, and the boxes correspond to systematical uncertainties from the data.

effects smaller in such collisions. In p-Pb collisions, an event with a high multiplicity value similar to those in pp collisions can come from the superposition of a few soft nucleon-nucleon collisions. Therefore, for similar multiplicity, the hardness of the event is not the same in the two systems.

The self-normalised yield of electrons from heavy-flavour hadron decays is compared in figure 16 with EPOS 2.592 simulations [117, 178]. The measurements in two p_T intervals are compared with the EPOS model without the hydrodynamic component, as provided by the authors. The EPOS model shows no p_T dependence similar to the observations in the data, but underpredicts the data at high multiplicity, showing an almost linear increase.

The self-normalised electron yields in p-Pb collisions in different p_T ranges are also compared with the normalised yields of D mesons [111] in p-Pb collisions at $\sqrt{s_{NN}}$ = 5.02 TeV in figure 17. Similar to the observation in pp collisions, the self-normalised yield of electrons from heavy-flavour hadron decays as a function of the self-normalised multiplicity shows a trend compatible with the one of D mesons. Also the multiplicity dependence of D meson yields in p-Pb collisions does not show a p_T dependence, which gives a hint that the production mechanisms of charm and beauty as a function of the multiplicity in p-Pb collisions are similar.

7 Summary

Heavy-flavour production at midrapidity was studied using electrons from heavy-flavour hadron decays in pp collisions at $\sqrt{s}$ = 13 TeV and in p-Pb collisions at $\sqrt{s_{NN}}$ = 8.16 TeV

JHEP08(2023)006

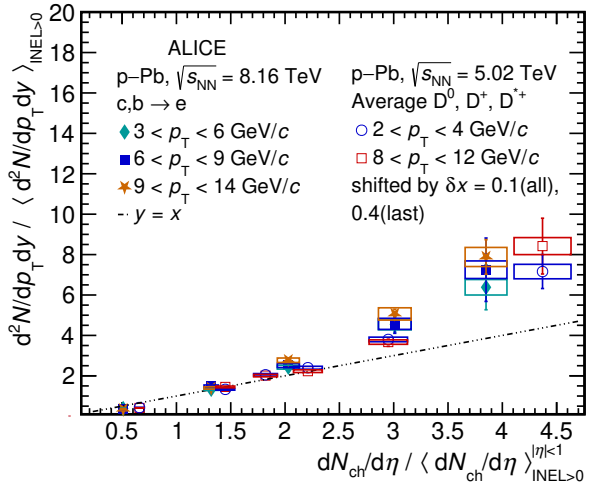

Figure 17. Self-normalised yields of electrons from heavy-flavour hadron decays measured in p-Pb collisions at $\sqrt{s_{\rm NN}} = 8.16$ TeV for different $p_{\rm T}$ intervals compared with self-normalised yields of D mesons in p-Pb collisions at $\sqrt{s_{\rm NN}} = 5.02$ TeV. The position of the points for p-Pb collisions at $\sqrt{s_{\rm NN}} = 5.02$ TeV on the x-axis are shifted horizontally by δx to improve the visibility.

with the ALICE detector at the LHC. The $p_{\rm T}$-differential production cross section of electrons from heavy-flavour hadron decays in pp collisions was compared with FONLL and GM-VFNS (b → B → D → e, b → B → e, c → D → e) pQCD calculations. The data are observed to lie on the upper edge of the FONLL uncertainties. The GM-VFNS calculation underestimates the cross section at low $p_{\rm T}$ but describes the data within the uncertainties for $p_{\rm T} > 5$ GeV/c. The nuclear modification factor in p-Pb collisions, $R_{\rm pPb}$, was computed and is consistent with unity within the statistical and systematic uncertainties. The $R_{\rm pPb}$ measurement shows no effects that could signal the formation of a hot medium and no significant cold nuclear matter effects within the uncertainties of the data in the measured $p_{\rm T}$ range. The $R_{\rm pPb}$ at $\sqrt{s_{\rm NN}} = 8.16$ TeV is consistent with that measured at $\sqrt{s_{\rm NN}} = 5.02$ TeV.

The multiplicity-dependent production of electrons from heavy-flavour hadron decays was measured using the self-normalised yield as a function of self-normalised charged-particle pseudorapidity density at midrapidity in pp and p-Pb collisions as a function of transverse momentum. A faster than linear increase was observed in both pp and p-Pb collisions. While in p-Pb collisions, no $p_{\rm T}$ dependence is observed within uncertainties, in pp collisions a strong $p_{\rm T}$ dependence is seen with high-$p_{\rm T}$ electrons showing a faster increase as a function of the self-normalised multiplicity. The measurement of self-normalised yield of electrons from heavy-flavour hadron decays in pp collisions was compared with PYTHIA 8.2 and EPOS 3 simulations, which describe the data. The measurement in p-Pb collisions was compared with the EPOS 2.592 model without hydrodynamics, which underestimates the data. The comparison of self-normalised yields of heavy-flavour and light-flavour particles show a similar stronger than linearly increasing trend in both colliding systems. In pp collisions the stronger than linear increase of heavy-flavour particles is mainly driven by auto-correlation effects which are independent of particle species, whereas in the case of

JHEP08(2023)006

p-Pb collisions, it is difficult to draw any conclusion since the multiplicity dependence of heavy-flavour production is also largely affected by the presence of multiple binary nucleon-nucleon interactions.

Acknowledgments

The ALICE Collaboration would like to thank all its engineers and technicians for their invaluable contributions to the construction of the experiment and the CERN accelerator teams for the outstanding performance of the LHC complex. The ALICE Collaboration gratefully acknowledges the resources and support provided by all Grid centres and the Worldwide LHC Computing Grid (WLCG) collaboration. The ALICE Collaboration acknowledges the following funding agencies for their support in building and running the ALICE detector: A. I. Alikhanyan National Science Laboratory (Yerevan Physics Institute) Foundation (ANSL), State Committee of Science and World Federation of Scientists (WFS), Armenia; Austrian Academy of Sciences, Austrian Science Fund (FWF): [M 2467-N36] and Nationalstiftung für Forschung, Technologie und Entwicklung, Austria; Ministry of Communications and High Technologies, National Nuclear Research Center, Azerbaijan; Conselho Nacional de Desenvolvimento Científico e Tecnológico (CNPq), Financiadora de Estudos e Projetos (Finep), Fundação de Amparo à Pesquisa do Estado de São Paulo (FAPESP) and Universidade Federal do Rio Grande do Sul (UFRGS), Brazil; Bulgarian Ministry of Education and Science, within the National Roadmap for Research Infrastructures 2020–2027 (object CERN), Bulgaria; Ministry of Education of China (MOEC), Ministry of Science & Technology of China (MSTC) and National Natural Science Foundation of China (NSFC), China; Ministry of Science and Education and Croatian Science Foundation, Croatia; Centro de Aplicaciones Tecnológicas y Desarrollo Nuclear (CEADEN), Cubaenergía, Cuba; Ministry of Education, Youth and Sports of the Czech Republic, Czech Republic; The Danish Council for Independent Research | Natural Sciences, the VILLUM FONDEN and Danish National Research Foundation (DNRF), Denmark; Helsinki Institute of Physics (HIP), Finland; Commissariat à l'Energie Atomique (CEA) and Institut National de Physique Nucléaire et de Physique des Particules (IN2P3) and Centre National de la Recherche Scientifique (CNRS), France; Bundesministerium für Bildung und Forschung (BMBF) and GSI Helmholtzzentrum für Schwerionenforschung GmbH, Germany; General Secretariat for Research and Technology, Ministry of Education, Research and Religions, Greece; National Research, Development and Innovation Office, Hungary; Department of Atomic Energy Government of India (DAE), Department of Science and Technology, Government of India (DST), University Grants Commission, Government of India (UGC) and Council of Scientific and Industrial Research (CSIR), India; National Research and Innovation Agency — BRIN, Indonesia; Istituto Nazionale di Fisica Nucleare (INFN), Italy; Japanese Ministry of Education, Culture, Sports, Science and Technology (MEXT) and Japan Society for the Promotion of Science (JSPS) KAKENHI, Japan; Consejo Nacional de Ciencia (CONACYT) y Tecnología, through Fondo de Cooperación Internacional en Ciencia y Tecnología (FONCICYT) and Dirección General de Asuntos del Personal Academico (DGAPA), Mexico; Nederlandse Organisatie voor Wetenschappelijk Onderzoek (NWO),

JHEP08(2023)006

Netherlands; The Research Council of Norway, Norway; Commission on Science and Technology for Sustainable Development in the South (COMSATS), Pakistan; Pontificia Universidad Católica del Perú, Peru; Ministry of Education and Science, National Science Centre and WUT ID-UB, Poland; Korea Institute of Science and Technology Information and National Research Foundation of Korea (NRF), Republic of Korea; Ministry of Education and Scientific Research, Institute of Atomic Physics, Ministry of Research and Innovation and Institute of Atomic Physics and University Politehnica of Bucharest, Romania; Ministry of Education, Science, Research and Sport of the Slovak Republic, Slovakia; National Research Foundation of South Africa, South Africa; Swedish Research Council (VR) and Knut & Alice Wallenberg Foundation (KAW), Sweden; European Organization for Nuclear Research, Switzerland; Suranaree University of Technology (SUT), National Science and Technology Development Agency (NSTDA), Thailand Science Research and Innovation (TSRI) and National Science, Research and Innovation Fund (NSRF), Thailand; Turkish Energy, Nuclear and Mineral Research Agency (TENMAK), Turkey; National Academy of Sciences of Ukraine, Ukraine; Science and Technology Facilities Council (STFC), United Kingdom; National Science Foundation of the United States of America (NSF) and United States Department of Energy, Office of Nuclear Physics (DOE NP), United States of America. In addition, individual groups or members have received support from: European Research Council, Strong 2020 — Horizon 2020 (grant nos. 950692, 824093), European Union; Academy of Finland (Center of Excellence in Quark Matter) (grant nos. 346327, 346328), Finland; DST-DAAD Project-based Personnel Exchange Programme, India; Programa de Apoyos para la Superación del Personal Académico, UNAM, Mexico.

JHEP08(2023)006

References

[1] B.A. Kniehl, G. Kramer, I. Schienbein and H. Spiesberger, *Finite-mass effects on inclusive B meson hadroproduction*, *Phys. Rev. D* **77** (2008) 014011 [arXiv:0705.4392] [INSPIRE].

[2] M. Cacciari et al., *QCD analysis of first b cross-section data at* 1.96 *TeV*, *JHEP* **07** (2004) 033 [hep-ph/0312132] [INSPIRE].

[3] B.A. Kniehl, G. Kramer, I. Schienbein and H. Spiesberger, *Collinear subtractions in hadroproduction of heavy quarks*, *Eur. Phys. J. C* **41** (2005) 199 [hep-ph/0502194] [INSPIRE].

[4] M. Cacciari and P. Nason, *Charm cross-sections for the Tevatron run II*, *JHEP* **09** (2003) 006 [hep-ph/0306212] [INSPIRE].

[5] ATLAS collaboration, *Measurement of $D^{*\pm}$, $D^{\pm}$ and $D_s^{\pm}$ meson production cross sections in pp collisions at $\sqrt{s} = 7$ TeV with the ATLAS detector*, *Nucl. Phys. B* **907** (2016) 717 [arXiv:1512.02913] [INSPIRE].

[6] ALICE collaboration, *Measurement of D^0 , D^+ , D^{*+} and D_s^+ production in pp collisions at $\sqrt{s} = 5.02$ TeV with ALICE*, *Eur. Phys. J. C* **79** (2019) 388 [arXiv:1901.07979] [INSPIRE].

[7] ALICE collaboration, *Heavy flavour decay muon production at forward rapidity in proton-proton collisions at* $\sqrt{s} = 7$ *TeV*, *Phys. Lett. B* **708** (2012) 265 [arXiv:1201.3791] [INSPIRE].

[8] ALICE collaboration, *Measurement of charm production at central rapidity in proton-proton collisions at* $\sqrt{s} = 2.76$ *TeV*, *JHEP* **07** (2012) 191 [arXiv:1205.4007] [INSPIRE].

[9] ALICE collaboration, *Measurement of electrons from semileptonic heavy-flavour hadron decays in pp collisions at* $\sqrt{s} = 7$ *TeV*, *Phys. Rev. D* **86** (2012) 112007 [arXiv:1205.5423] [INSPIRE].

[10] LHCb collaboration, *Measurements of prompt charm production cross-sections in pp collisions at* $\sqrt{s} = 5$ *TeV*, *JHEP* **06** (2017) 147 [arXiv:1610.02230] [INSPIRE].

[11] CMS collaboration, *Nuclear modification factor of* D^0 *mesons in PbPb collisions at* $\sqrt{s_{\rm NN}} = 5.02$ *TeV*, *Phys. Lett. B* **782** (2018) 474 [arXiv:1708.04962] [INSPIRE].

[12] LHCb collaboration, *Measurements of prompt charm production cross-sections in pp collisions at* $\sqrt{s} = 5$ *TeV*, *JHEP* **06** (2017) 147 [arXiv:1610.02230] [INSPIRE].

[13] LHCb collaboration, *Measurements of prompt charm production cross-sections in pp collisions at* $\sqrt{s} = 13$ *TeV*, *JHEP* **03** (2016) 159 [*Erratum ibid.* **09** (2016) 013] [arXiv:1510.01707] [INSPIRE].

[14] ALICE collaboration, *Observation of a multiplicity dependence in the* p_T*-differential charm baryon-to-meson ratios in proton-proton collisions at* $\sqrt{s} = 13$ *TeV*, *Phys. Lett. B* **829** (2022) 137065 [arXiv:2111.11948] [INSPIRE].

[15] ALICE collaboration, *Measurement of electrons from beauty hadron decays in pp collisions at* $\sqrt{s} = 7$ *TeV*, *Phys. Lett. B* **721** (2013) 13 [arXiv:1208.1902] [INSPIRE].

[16] ALICE collaboration, *Measurement of electrons from semileptonic heavy-flavour hadron decays at midrapidity in pp and Pb-Pb collisions at* $\sqrt{s_{\rm NN}} = 5.02$ *TeV*, *Phys. Lett. B* **804** (2020) 135377 [arXiv:1910.09110] [INSPIRE].

[17] ATLAS collaboration, *Measurement of the nuclear modification factor for muons from charm and bottom hadrons in Pb+Pb collisions at* 5.02 *TeV with the ATLAS detector*, *Phys. Lett. B* **829** (2022) 137077 [arXiv:2109.00411] [INSPIRE].

[18] ALICE collaboration, *Measurement of prompt* J/ψ *and beauty hadron production cross sections at mid-rapidity in pp collisions at* $\sqrt{s} = 7$ *TeV*, *JHEP* **11** (2012) 065 [arXiv:1205.5880] [INSPIRE].

[19] ALICE collaboration, *Measurement of electrons from beauty-hadron decays in p-Pb collisions at* $\sqrt{s_{\rm NN}} = 5.02$ *TeV and Pb-Pb collisions at* $\sqrt{s_{\rm NN}} = 2.76$ *TeV*, *JHEP* **07** (2017) 052 [arXiv:1609.03898] [INSPIRE].

[20] ATLAS collaboration, *Measurement of the differential cross-section of* B^+ *meson production in pp collisions at* $\sqrt{s} = 7$ *TeV at ATLAS*, *JHEP* **10** (2013) 042 [arXiv:1307.0126] [INSPIRE].

[21] CMS collaboration, *Prompt and non-prompt* J/ψ *production in pp collisions at* $\sqrt{s} = 7$ *TeV*, *Eur. Phys. J. C* **71** (2011) 1575 [arXiv:1011.4193] [INSPIRE].

[22] LHCb collaboration, *Measurement of* $\sigma(pp \to b\bar{b}X)$ *at* $\sqrt{s} = 7$ *TeV in the forward region*, *Phys. Lett. B* **694** (2010) 209 [arXiv:1009.2731] [INSPIRE].

JHEP08(2023)006

[23] ALICE collaboration, *Measurement of beauty and charm production in pp collisions at $\sqrt{s} = 5.02$ TeV via non-prompt and prompt D mesons*, *JHEP* **05** (2021) 220 [arXiv:2102.13601] [INSPIRE].

[24] ALICE collaboration, *Dielectron production in proton-proton and proton-lead collisions at $\sqrt{s_{\rm NN}} = 5.02$ TeV*, *Phys. Rev. C* **102** (2020) 055204 [arXiv:2005.11995] [INSPIRE].

[25] CMS collaboration, *Measurement of the total and differential inclusive B^+ hadron cross sections in pp collisions at $\sqrt{s} = 13$ TeV*, *Phys. Lett. B* **771** (2017) 435 [arXiv:1609.00873] [INSPIRE].

[26] LHCb collaboration, *Measurement of the b-quark production cross-section in 7 and 13 TeV pp collisions*, *Phys. Rev. Lett.* **118** (2017) 052002 [*Erratum ibid.* **119** (2017) 169901] [arXiv:1612.05140] [INSPIRE].

[27] LHCb collaboration, *Measurement of forward J/ψ production cross-sections in pp collisions at $\sqrt{s} = 13$ TeV*, *JHEP* **10** (2015) 172 [*Erratum ibid.* **05** (2017) 063] [arXiv:1509.00771] [INSPIRE].

[28] ALICE collaboration, *Measurement of electrons from beauty hadron decays in pp collisions at $\sqrt{s} = 7$ TeV*, *Phys. Lett. B* **721** (2013) 13 [arXiv:1208.1902] [INSPIRE].

[29] B.A. Kniehl, *Inclusive production of heavy-flavored hadrons at NLO in the GM-VFNS*, in the proceedings of the 16th *International Workshop on Deep Inelastic Scattering and Related Subjects*, (2008), p. 195 [DOI:10.3360/dis.2008.195] [arXiv:0807.2215] [INSPIRE].

[30] B.A. Kniehl, G. Kramer, I. Schienbein and H. Spiesberger, *Inclusive B-meson production at the LHC in the GM-VFN scheme*, *Phys. Rev. D* **84** (2011) 094026 [arXiv:1109.2472] [INSPIRE].

[31] B.A. Kniehl, G. Kramer, I. Schienbein and H. Spiesberger, *Reconciling open charm production at the Fermilab Tevatron with QCD*, *Phys. Rev. Lett.* **96** (2006) 012001 [hep-ph/0508129] [INSPIRE].

[32] P. Bolzoni and G. Kramer, *Inclusive lepton production from heavy-hadron decay in pp collisions at the LHC*, *Nucl. Phys. B* **872** (2013) 253 [arXiv:1212.4356] [INSPIRE].

[33] P. Bolzoni and G. Kramer, *Inclusive charmed-meson production from bottom hadron decays at the LHC*, *J. Phys. G* **41** (2014) 075006 [arXiv:1310.2924] [INSPIRE].

[34] M. Cacciari et al., *Theoretical predictions for charm and bottom production at the LHC*, *JHEP* **10** (2012) 137 [arXiv:1205.6344] [INSPIRE].

[35] ALICE collaboration, *Λ_c^+ production in pp collisions at $\sqrt{s} = 7$ TeV and in p-Pb collisions at $\sqrt{s_{\rm NN}} = 5.02$ TeV*, *JHEP* **04** (2018) 108 [arXiv:1712.09581] [INSPIRE].

[36] ALICE collaboration, *Λ_c^+ production and baryon-to-meson ratios in pp and p-Pb collisions at $\sqrt{s_{\rm NN}} = 5.02$ TeV at the LHC*, *Phys. Rev. Lett.* **127** (2021) 202301 [arXiv:2011.06078] [INSPIRE].

[37] ALICE collaboration, *Λ_c^+ production in pp and in p-Pb collisions at $\sqrt{s_{\rm NN}} = 5.02$ TeV*, *Phys. Rev. C* **104** (2021) 054905 [arXiv:2011.06079] [INSPIRE].

[38] CMS collaboration, *Production of Λ_c^+ baryons in proton-proton and lead-lead collisions at $\sqrt{s_{\rm NN}} = 5.02$ TeV*, *Phys. Lett. B* **803** (2020) 135328 [arXiv:1906.03322] [INSPIRE].

[39] ALICE collaboration, *First measurement of Ξ_c^0 production in pp collisions at $\sqrt{s} = 7$ TeV*, *Phys. Lett. B* **781** (2018) 8 [arXiv:1712.04242] [INSPIRE].

JHEP08(2023)006

[40] ALICE collaboration, *Measurement of the production cross section of prompt Ξ_c^0 baryons at midrapidity in pp collisions at $\sqrt{s} = 5.02$ TeV*, *JHEP* **10** (2021) 159 [arXiv:2105.05616] [INSPIRE].

[41] ALICE collaboration, *Measurement of the cross sections of Ξ_c^0 and Ξ_c^+ baryons and of the branching-fraction ratio $BR(\Xi_c^0 \to \Xi^- e^+ \nu_e)/BR(\Xi_c^0 \to \Xi^- \pi^+)$ in pp collisions at 13 TeV*, *Phys. Rev. Lett.* **127** (2021) 272001 [arXiv:2105.05187] [INSPIRE].

[42] ALICE collaboration, *Measurement of prompt D^0, Λ_c^+, and $\Sigma_c^{0,++}(2455)$ production in proton-proton collisions at $\sqrt{s} = 13$ TeV*, *Phys. Rev. Lett.* **128** (2022) 012001 [arXiv:2106.08278] [INSPIRE].

[43] ALICE collaboration, *First measurement of Ω_c^0 production in pp collisions at $\sqrt{s} = 13$ TeV*, arXiv:2205.13993 [INSPIRE].

[44] L. Gladilin, *Fragmentation fractions of c and b quarks into charmed hadrons at LEP*, *Eur. Phys. J. C* **75** (2015) 19 [arXiv:1404.3888] [INSPIRE].

[45] CDF collaboration, *Measurement of ratios of fragmentation fractions for bottom hadrons in $p\bar{p}$ collisions at $\sqrt{s} = 1.96$ TeV*, *Phys. Rev. D* **77** (2008) 072003 [arXiv:0801.4375] [INSPIRE].

[46] LHCb collaboration, *Measurement of b-hadron production fractions in 7 TeV pp collisions*, *Phys. Rev. D* **85** (2012) 032008 [arXiv:1111.2357] [INSPIRE].

[47] LHCb collaboration, *Measurement of b hadron fractions in 13 TeV pp collisions*, *Phys. Rev. D* **100** (2019) 031102 [arXiv:1902.06794] [INSPIRE].

[48] K.J. Eskola, H. Paukkunen and C.A. Salgado, *EPS09: a new generation of NLO and LO nuclear parton distribution functions*, *JHEP* **04** (2009) 065 [arXiv:0902.4154] [INSPIRE].

[49] D. de Florian and R. Sassot, *Nuclear parton distributions at next-to-leading order*, *Phys. Rev. D* **69** (2004) 074028 [hep-ph/0311227] [INSPIRE].

[50] M. Hirai, S. Kumano and T.-H. Nagai, *Determination of nuclear parton distribution functions and their uncertainties in next-to-leading order*, *Phys. Rev. C* **76** (2007) 065207 [arXiv:0709.3038] [INSPIRE].

[51] K.J. Eskola, P. Paakkinen, H. Paukkunen and C.A. Salgado, *EPPS16: nuclear parton distributions with LHC data*, *Eur. Phys. J. C* **77** (2017) 163 [arXiv:1612.05741] [INSPIRE].

[52] H. Fujii and K. Watanabe, *Heavy quark pair production in high energy pA collisions: open heavy flavors*, *Nucl. Phys. A* **920** (2013) 78 [arXiv:1308.1258] [INSPIRE].

[53] P. Tribedy and R. Venugopalan, *QCD saturation at the LHC: comparisons of models to p+p and A+A data and predictions for p+Pb collisions*, *Phys. Lett. B* **710** (2012) 125 [arXiv:1112.2445] [INSPIRE].

[54] J.L. Albacete, A. Dumitru, H. Fujii and Y. Nara, *CGC predictions for p+Pb collisions at the LHC*, *Nucl. Phys. A* **897** (2013) 1 [arXiv:1209.2001] [INSPIRE].

[55] A.H. Rezaeian, *CGC predictions for p+A collisions at the LHC and signature of QCD saturation*, *Phys. Lett. B* **718** (2013) 1058 [arXiv:1210.2385] [INSPIRE].

[56] M. Lev and B. Petersson, *Nuclear effects at large transverse momentum in a QCD parton model*, *Z. Phys. C* **21** (1983) 155 [INSPIRE].

[57] B.Z. Kopeliovich, J. Nemchik, A. Schafer and A.V. Tarasov, *Cronin effect in hadron production off nuclei*, *Phys. Rev. Lett.* **88** (2002) 232303 [hep-ph/0201010] [INSPIRE].

JHEP08(2023)006

[58] I. Vitev, *Non-Abelian energy loss in cold nuclear matter*, *Phys. Rev. C* **75** (2007) 064906 [hep-ph/0703002] [INSPIRE].

[59] ALICE collaboration, *Measurement of electrons from heavy-flavour hadron decays in p-Pb collisions at* $\sqrt{s_{\rm NN}} = 5.02$ *TeV*, *Phys. Lett. B* **754** (2016) 81 [arXiv:1509.07491] [INSPIRE].

[60] ALICE collaboration, *Measurement of prompt* D^0, D^+, D^{*+}, *and* $D_{\rm S}^+$ *production in p-Pb collisions at* $\sqrt{s_{\rm NN}} = 5.02$ *TeV*, *JHEP* **12** (2019) 092 [arXiv:1906.03425] [INSPIRE].

[61] ALICE collaboration, *Inclusive, prompt and non-prompt* J/ψ *production at midrapidity in p-Pb collisions at* $\sqrt{s_{\rm NN}} = 5.02$ *TeV*, *JHEP* **06** (2022) 011 [arXiv:2105.04957] [INSPIRE].

[62] ALICE collaboration, J/ψ *production at midrapidity in p-Pb collisions at* $\sqrt{s_{\rm NN}} = 8.16$ *TeV*, arXiv:2211.14153 [INSPIRE].

[63] ALICE collaboration, *Inclusive* J/ψ *production at forward and backward rapidity in p-Pb collisions at* $\sqrt{s_{\rm NN}} = 8.16$ *TeV*, *JHEP* **07** (2018) 160 [arXiv:1805.04381] [INSPIRE].

[64] ALICE collaboration, *Measurement of prompt D-meson production in p-Pb collisions at* $\sqrt{s_{\rm NN}} = 5.02$ *TeV*, *Phys. Rev. Lett.* **113** (2014) 232301 [arXiv:1405.3452] [INSPIRE].

[65] ALICE collaboration, *First measurement of* Λ_c^+ *production down to* $p_T = 0$ *in pp and p-Pb collisions at* $\sqrt{s_{\rm NN}} = 5.02$ *TeV*, *Phys. Rev. C* **107** (2023) 064901 [arXiv:2211.14032] [INSPIRE].

[66] ATLAS collaboration, *Measurement of quarkonium production in proton-lead and proton-proton collisions at* 5.02 *TeV with the ATLAS detector*, *Eur. Phys. J. C* **78** (2018) 171 [arXiv:1709.03089] [INSPIRE].

[67] CMS collaboration, *Measurement of prompt and nonprompt* J/ψ *production in pp and pPb collisions at* $\sqrt{s_{\rm NN}} = 5.02$ *TeV*, *Eur. Phys. J. C* **77** (2017) 269 [arXiv:1702.01462] [INSPIRE].

[68] CMS collaboration, *Study of B meson production in p+Pb collisions at* $\sqrt{s_{\rm NN}} = 5.02$ *TeV using exclusive hadronic decays*, *Phys. Rev. Lett.* **116** (2016) 032301 [arXiv:1508.06678] [INSPIRE].

[69] LHCb collaboration, *Study of* J/ψ *production and cold nuclear matter effects in pPb collisions at* $\sqrt{s_{\rm NN}} = 5$ *TeV*, *JHEP* **02** (2014) 072 [arXiv:1308.6729] [INSPIRE].

[70] LHCb collaboration, *Prompt and nonprompt* J/ψ *production and nuclear modification in pPb collisions at* $\sqrt{s_{NN}} = 8.16$ *TeV*, *Phys. Lett. B* **774** (2017) 159 [arXiv:1706.07122] [INSPIRE].

[71] LHCb collaboration, *Measurement of* B^+, B^0 *and* Λ_b^0 *production in pPb collisions at* $\sqrt{s_{\rm NN}} = 8.16$ *TeV*, *Phys. Rev. D* **99** (2019) 052011 [arXiv:1902.05599] [INSPIRE].

[72] LHCb collaboration, *Measurement of the prompt* D^0 *nuclear modification factor in pPb collisions at* $\sqrt{s_{\rm NN}} = 8.16$ *TeV*, arXiv:2205.03936 [INSPIRE].

[73] CMS collaboration, *Observation of long-range near-side angular correlations in proton-proton collisions at the LHC*, *JHEP* **09** (2010) 091 [arXiv:1009.4122] [INSPIRE].

[74] ATLAS collaboration, *Observation of long-range elliptic azimuthal anisotropies in* $\sqrt{s} = 13$ *and* 2.76 *TeV pp collisions with the ATLAS detector*, *Phys. Rev. Lett.* **116** (2016) 172301 [arXiv:1509.04776] [INSPIRE].

[75] CMS collaboration, *Measurement of long-range near-side two-particle angular correlations in pp collisions at* $\sqrt{s} = 13$ *TeV*, *Phys. Rev. Lett.* **116** (2016) 172302 [arXiv:1510.03068] [INSPIRE].

JHEP08(2023)006

[76] ALICE collaboration, *Long-range angular correlations on the near and away side in p-Pb collisions at* $\sqrt{s_{\rm NN}} = 5.02$ *TeV*, *Phys. Lett. B* **719** (2013) 29 [arXiv:1212.2001] [INSPIRE].

[77] ATLAS collaboration, *Measurements of long-range azimuthal anisotropies and associated Fourier coefficients for pp collisions at* $\sqrt{s} = 5.02$ *and* 13 *TeV and p+Pb collisions at* $\sqrt{s_{\rm NN}} = 5.02$ *TeV with the ATLAS detector*, *Phys. Rev. C* **96** (2017) 024908 [arXiv:1609.06213] [INSPIRE].

[78] CMS collaboration, *Multiplicity and transverse momentum dependence of two- and four-particle correlations in pPb and PbPb collisions*, *Phys. Lett. B* **724** (2013) 213 [arXiv:1305.0609] [INSPIRE].

[79] ALICE collaboration, *Long-range angular correlations of* π, K *and* p *in p-Pb collisions at* $\sqrt{s_{\rm NN}} = 5.02$ *TeV*, *Phys. Lett. B* **726** (2013) 164 [arXiv:1307.3237] [INSPIRE].

[80] CMS collaboration, *Long-range two-particle correlations of strange hadrons with charged particles in pPb and PbPb collisions at LHC energies*, *Phys. Lett. B* **742** (2015) 200 [arXiv:1409.3392] [INSPIRE].

[81] PHENIX collaboration, *Quadrupole anisotropy in dihadron azimuthal correlations in central d+Au collisions at* $\sqrt{s_{\rm NN}} = 200$ *GeV*, *Phys. Rev. Lett.* **111** (2013) 212301 [arXiv:1303.1794] [INSPIRE].

[82] STAR collaboration, *Long-range pseudorapidity dihadron correlations in d+Au collisions at* $\sqrt{s_{\rm NN}} = 200$ *GeV*, *Phys. Lett. B* **747** (2015) 265 [arXiv:1502.07652] [INSPIRE].

[83] PHENIX collaboration, *Measurements of elliptic and triangular flow in high-multiplicity* ^{3}*He+Au collisions at* $\sqrt{s_{\rm NN}} = 200$ *GeV*, *Phys. Rev. Lett.* **115** (2015) 142301 [arXiv:1507.06273] [INSPIRE].

[84] CMS collaboration, *Observation of long-range near-side angular correlations in proton-proton collisions at the LHC*, *JHEP* **09** (2010) 091 [arXiv:1009.4122] [INSPIRE].

[85] CMS collaboration, *Observation of long-range near-side angular correlations in proton-lead collisions at the LHC*, *Phys. Lett. B* **718** (2013) 795 [arXiv:1210.5482] [INSPIRE].

[86] ALICE collaboration, *Long-range angular correlations on the near and away side in p-Pb collisions at* $\sqrt{s_{\rm NN}} = 5.02$ *TeV*, *Phys. Lett. B* **719** (2013) 29 [arXiv:1212.2001] [INSPIRE].

[87] ATLAS collaboration, *Observation of associated near-side and away-side long-range correlations in* $\sqrt{s_{\rm NN}} = 5.02$ *TeV proton-lead collisions with the ATLAS detector*, *Phys. Rev. Lett.* **110** (2013) 182302 [arXiv:1212.5198] [INSPIRE].

[88] LHCb collaboration, *Measurements of long-range near-side angular correlations in* $\sqrt{s_{NN}} = 5$ *TeV proton-lead collisions in the forward region*, *Phys. Lett. B* **762** (2016) 473 [arXiv:1512.00439] [INSPIRE].

[89] ALICE collaboration, *Azimuthal anisotropy of heavy-flavor decay electrons in p-Pb collisions at* $\sqrt{s_{\rm NN}} = 5.02$ *TeV*, *Phys. Rev. Lett.* **122** (2019) 072301 [arXiv:1805.04367] [INSPIRE].

[90] CMS collaboration, *Elliptic flow of charm and strange hadrons in high-multiplicity pPb collisions at* $\sqrt{s_{\rm NN}} = 8.16$ *TeV*, *Phys. Rev. Lett.* **121** (2018) 082301 [arXiv:1804.09767] [INSPIRE].

[91] CMS collaboration, *Observation of prompt* J/ψ *meson elliptic flow in high-multiplicity pPb collisions at* $\sqrt{s_{\rm NN}} = 8.16$ *TeV*, *Phys. Lett. B* **791** (2019) 172 [arXiv:1810.01473] [INSPIRE].

JHEP08(2023)006

[92] ALICE collaboration, *Search for collectivity with azimuthal J/ψ-hadron correlations in high multiplicity p-Pb collisions at $\sqrt{s_{\rm NN}} = 5.02$ and 8.16 TeV*, *Phys. Lett. B* **780** (2018) 7 [arXiv:1709.06807] [INSPIRE].

[93] CMS collaboration, *Studies of charm and beauty hadron long-range correlations in pp and pPb collisions at LHC energies*, *Phys. Lett. B* **813** (2021) 136036 [arXiv:2009.07065] [INSPIRE].

[94] ALICE collaboration, *The ALICE experiment — a journey through QCD*, arXiv:2211.04384 [INSPIRE].

[95] K. Werner, I. Karpenko and T. Pierog, *The 'ridge' in proton-proton scattering at 7 TeV*, *Phys. Rev. Lett.* **106** (2011) 122004 [arXiv:1011.0375] [INSPIRE].

[96] W.-T. Deng, Z. Xu and C. Greiner, *Elliptic and triangular flow and their correlation in ultrarelativistic high multiplicity proton proton collisions at 14 TeV*, *Phys. Lett. B* **711** (2012) 301 [arXiv:1112.0470] [INSPIRE].

[97] K. Werner et al., *Evidence for flow from hydrodynamic simulations of p-Pb collisions at 5.02 TeV from ν_2 mass splitting*, *Phys. Rev. Lett.* **112** (2014) 232301 [arXiv:1307.4379] [INSPIRE].

[98] B. Schenke, C. Shen and P. Tribedy, *Hybrid color glass condensate and hydrodynamic description of the relativistic heavy ion collider small system scan*, *Phys. Lett. B* **803** (2020) 135322 [arXiv:1908.06212] [INSPIRE].

[99] C. Bierlich, G. Gustafson, L. Lönnblad and A. Tarasov, *Effects of overlapping strings in pp collisions*, *JHEP* **03** (2015) 148 [arXiv:1412.6259] [INSPIRE].

[100] I. Bautista, A.F. Téllez and P. Ghosh, *Indication of change of phase in high-multiplicity proton-proton events at LHC in string percolation model*, *Phys. Rev. D* **92** (2015) 071504 [arXiv:1509.02278] [INSPIRE].

[101] T. Sjöstrand et al., *An introduction to PYTHIA 8.2*, *Comput. Phys. Commun.* **191** (2015) 159 [arXiv:1410.3012] [INSPIRE].

[102] A. Ortiz Velasquez et al., *Color reconnection and flowlike patterns in pp collisions*, *Phys. Rev. Lett.* **111** (2013) 042001 [arXiv:1303.6326] [INSPIRE].

[103] J.D. Orjuela Koop, A. Adare, D. McGlinchey and J.L. Nagle, *Azimuthal anisotropy relative to the participant plane from a multiphase transport model in central p+Au , d+Au, and ^{3}He+Au collisions at $\sqrt{s_{\rm NN}} = 200$ GeV*, *Phys. Rev. C* **92** (2015) 054903 [arXiv:1501.06880] [INSPIRE].

[104] S. Schlichting and P. Tribedy, *Collectivity in small collision systems: an initial-state perspective*, *Adv. High Energy Phys.* **2016** (2016) 8460349 [arXiv:1611.00329] [INSPIRE].

[105] B. Schenke, S. Schlichting, P. Tribedy and R. Venugopalan, *Mass ordering of spectra from fragmentation of saturated gluon states in high multiplicity proton-proton collisions*, *Phys. Rev. Lett.* **117** (2016) 162301 [arXiv:1607.02496] [INSPIRE].

[106] ALICE collaboration, *Measurement of charm and beauty production at central rapidity versus charged-particle multiplicity in proton-proton collisions at $\sqrt{s} = 7$ TeV*, *JHEP* **09** (2015) 148 [arXiv:1505.00664] [INSPIRE].

[107] ALICE collaboration, *Multiplicity dependence of J/ψ production at midrapidity in pp collisions at $\sqrt{s} = 13$ TeV*, *Phys. Lett. B* **810** (2020) 135758 [arXiv:2005.11123] [INSPIRE].

JHEP08(2023)006

[108] STAR collaboration, *J/ψ production cross section and its dependence on charged-particle multiplicity in p+p collisions at $\sqrt{s} = 200$ GeV*, *Phys. Lett. B* **786** (2018) 87 [arXiv:1805.03745] [INSPIRE].

[109] CMS collaboration, *Event activity dependence of $\Upsilon(nS)$ production in $\sqrt{s_{\rm NN}} = 5.02$ TeV pPb and $\sqrt{s} = 2.76$ TeV pp collisions*, *JHEP* **04** (2014) 103 [arXiv:1312.6300] [INSPIRE].

[110] ALICE collaboration, *J/ψ production as a function of charged-particle multiplicity in p-Pb collisions at $\sqrt{s_{\rm NN}} = 8.16$ TeV*, *JHEP* **09** (2020) 162 [arXiv:2004.12673] [INSPIRE].

[111] ALICE collaboration, *Measurement of D-meson production versus multiplicity in p-Pb collisions at $\sqrt{s_{\rm NN}} = 5.02$ TeV*, *JHEP* **08** (2016) 078 [arXiv:1602.07240] [INSPIRE].

[112] CMS collaboration, *Investigation into the event-activity dependence of $\Upsilon(nS)$ relative production in proton-proton collisions at $\sqrt{s} = 7$ TeV*, *JHEP* **11** (2020) 001 [arXiv:2007.04277] [INSPIRE].

[113] ALICE collaboration, *Multiplicity dependence of Υ production at forward rapidity in pp collisions at $\sqrt{s} = 13$ TeV*, arXiv:2209.04241 [INSPIRE].

[114] ALICE collaboration, *Charged-particle production as a function of multiplicity and transverse spherocity in pp collisions at $\sqrt{s} = 5.02$ and 13 TeV*, *Eur. Phys. J. C* **79** (2019) 857 [arXiv:1905.07208] [INSPIRE].

[115] ALICE collaboration, *Multiplicity dependence of light-flavor hadron production in pp collisions at $\sqrt{s} = 7$ TeV*, *Phys. Rev. C* **99** (2019) 024906 [arXiv:1807.11321] [INSPIRE].

[116] T. Sjostrand, S. Mrenna and P.Z. Skands, *PYTHIA* 6.4 *physics and manual*, *JHEP* **05** (2006) 026 [hep-ph/0603175] [INSPIRE].

[117] K. Werner, B. Guiot, I. Karpenko and T. Pierog, *Analysing radial flow features in p-Pb and p-p collisions at several TeV by studying identified particle production in EPOS3*, *Phys. Rev. C* **89** (2014) 064903 [arXiv:1312.1233] [INSPIRE].

[118] T. Pierog et al., *EPOS LHC: test of collective hadronization with data measured at the CERN Large Hadron Collider*, *Phys. Rev. C* **92** (2015) 034906 [arXiv:1306.0121] [INSPIRE].

[119] LHCb collaboration, *Evidence for modification of b quark hadronization in high-multiplicity pp collisions at $\sqrt{s} = 13$ TeV*, arXiv:2204.13042 [INSPIRE].

[120] ALICE collaboration, *The ALICE experiment at the CERN LHC*, 2008 *JINST* **3** S08002 [INSPIRE].

[121] ALICE collaboration, *Performance of the ALICE experiment at the CERN LHC*, *Int. J. Mod. Phys. A* **29** (2014) 1430044 [arXiv:1402.4476] [INSPIRE].

[122] ALICE collaboration, *ALICE technical design report of the inner tracking system (ITS)*, CERN-LHCC-99-012, CERN, Geneva, Switzerland (1999) [INSPIRE].

[123] ALICE collaboration, *ALICE time projection chamber: technical design report*, CERN-OPEN-2000-183, CERN, Geneva, Switzerland (2000).

[124] ALICE collaboration, *ALICE Time-Of-Flight system (TOF): technical design report*, CERN-LHCC-2000-012, CERN, Geneva, Switzerland (2000).

[125] ALICE collaboration, *ALICE Time-Of Flight system (TOF): addendum to the technical design report*, CERN-LHCC-2002-016, CERN, Geneva, Switzerland (2002).

[126] ALICE collaboration, *ALICE electromagnetic calorimeter technical design report*, CERN-LHCC-2008-014, CERN, Geneva, Switzerland (2008).

JHEP08(2023)006

[127] J. Allen et al., *ALICE DCal: an addendum to the EMCal technical design report di-jet and hadron-jet correlation measurements in ALICE*, CERN-LHCC-2010-011, CERN, Geneva, Switzerland (2010).

[128] E. Cerron Zeballos et al., *A new type of resistive plate chamber: the multigap RPC*, *Nucl. Instrum. Meth. A* **374** (1996) 132 [INSPIRE].

[129] ALICE collaboration, *ALICE forward detectors: FMD, TO and VO. Technical design report*, CERN-LHCC-2004-025, CERN, Geneva, Switzerland (2004).

[130] ALICE collaboration, *ALICE technical design report of the zero degree calorimeter (ZDC)*, CERN-LHCC-99-05, CERN, Geneva, Switzerland (1999) [INSPIRE].

[131] ALICE collaboration, *Performance of the ALICE electromagnetic calorimeter*, arXiv:2209.04216 [INSPIRE].

[132] ALICE collaboration, *ALICE luminosity determination for pp collisions at* $\sqrt{s} = 13$ *TeV*, ALICE-PUBLIC-2016-002, CERN, Geneva, Switzerland (2016).

[133] ALICE collaboration, *ALICE luminosity determination for p-Pb collisions at* $\sqrt{s_{\rm NN}} = 8.16$ *TeV*, ALICE-PUBLIC-2018-002, CERN, Geneva, Switzerland (2018).

[134] ALICE collaboration, *Pseudorapidity density of charged particles in p+Pb collisions at* $\sqrt{s_{\rm NN}} = 5.02$ *TeV*, *Phys. Rev. Lett.* **110** (2013) 032301 [arXiv:1210.3615] [INSPIRE].

[135] ALICE collaboration, *Charged-particle pseudorapidity density at mid-rapidity in p-Pb collisions at* $\sqrt{s_{\rm NN}} = 8.16$ *TeV*, *Eur. Phys. J. C* **79** (2019) 307 [arXiv:1812.01312] [INSPIRE].

[136] ALICE collaboration, *J/ψ production as a function of charged particle multiplicity in pp collisions at* $\sqrt{s} = 7$ *TeV*, *Phys. Lett. B* **712** (2012) 165 [arXiv:1202.2816] [INSPIRE].

[137] ALICE collaboration, *Pseudorapidity and transverse-momentum distributions of charged particles in proton-proton collisions at* $\sqrt{s} = 13$ *TeV*, *Phys. Lett. B* **753** (2016) 319 [arXiv:1509.08734] [INSPIRE].

[138] S. Roesler, R. Engel and J. Ranft, *The Monte Carlo event generator DPMJET-III*, in the proceedings of the *International conference on advanced Monte Carlo for radiation physics, particle transport simulation and applications (MC* 2000*)*, (2000), p. 1033 [DOI:10.1007/978-3-642-18211-2_166] [hep-ph/0012252] [INSPIRE].

[139] R. Brun et al., *GEANT: detector description and simulation tool; October* 1994, CERN-W-5013, CERN, Geneva, Switzerland (1993) [DOI:10.17181/CERN.MUHF.DMJ1].

[140] ALICE collaboration, *Pseudorapidity distributions of charged particles as a function of mid- and forward rapidity multiplicities in pp collisions at* $\sqrt{s} = 5.02$*,* 7 *and* 13 *TeV*, *Eur. Phys. J. C* **81** (2021) 630 [arXiv:2009.09434] [INSPIRE].

[141] ALICE collaboration, *Measurement of electrons from heavy-flavour hadron decays as a function of multiplicity in p-Pb collisions at* $\sqrt{s_{\rm NN}} = 5.02$ *TeV*, *JHEP* **02** (2020) 077 [arXiv:1910.14399] [INSPIRE].

[142] ALICE collaboration, *Measurement of electrons from semileptonic heavy-flavour hadron decays at midrapidity in pp and Pb-Pb collisions at* $\sqrt{s_{\rm NN}} = 5.02$ *TeV*, *Phys. Lett. B* **804** (2020) 135377 [arXiv:1910.09110] [INSPIRE].

[143] H. Bethe, *Theory of the passage of fast corpuscular rays through matter*, *Annalen Phys.* **5** (1930) 325 [INSPIRE].

[144] ALICE collaboration, *ALICE: physics performance report*, *J. Phys. G* **32** (2006) 1295 [INSPIRE].

JHEP08(2023)006

[145] T.C. Awes et al., *A simple method of shower localization and identification in laterally segmented calorimeters*, *Nucl. Instrum. Meth. A* **311** (1992) 130 [INSPIRE].

[146] ALICE collaboration, *Production of π^0 and η mesons up to high transverse momentum in pp collisions at 2.76 TeV*, *Eur. Phys. J. C* **77** (2017) 339 [arXiv:1702.00917] [INSPIRE].

[147] X.-N. Wang and M. Gyulassy, *HIJING: a Monte Carlo model for multiple jet production in pp, pA and AA collisions*, *Phys. Rev. D* **44** (1991) 3501 [INSPIRE].

[148] ALICE collaboration, *Production of light-flavor hadrons in pp collisions at $\sqrt{s} = 7$ and $\sqrt{s} = 13$ TeV*, *Eur. Phys. J. C* **81** (2021) 256 [arXiv:2005.11120] [INSPIRE].

[149] G. Gatoff and C.Y. Wong, *Origin of the soft p_T spectra*, *Phys. Rev. D* **46** (1992) 997 [INSPIRE].

[150] P.K. Khandai, P. Shukla and V. Singh, *Meson spectra and m_T scaling in p+p, d+Au, and Au+Au collisions at $\sqrt{s_{\rm NN}} = 200$ GeV*, *Phys. Rev. C* **84** (2011) 054904 [arXiv:1110.3929] [INSPIRE].

[151] L. Altenkämper, F. Bock, C. Loizides and N. Schmidt, *Applicability of transverse mass scaling in hadronic collisions at energies available at the CERN Large Hadron Collider*, *Phys. Rev. C* **96** (2017) 064907 [arXiv:1710.01933] [INSPIRE].

[152] ALICE collaboration, *Nuclear modification factor of light neutral-meson spectra up to high transverse momentum in p-Pb collisions at $\sqrt{s_{\rm NN}} = 8.16$ TeV*, *Phys. Lett. B* **827** (2022) 136943 [arXiv:2104.03116] [INSPIRE].

[153] ALICE collaboration, *Measurements of low-p_T electrons from semileptonic heavy-flavour hadron decays at mid-rapidity in pp and Pb-Pb collisions at $\sqrt{s_{\rm NN}} = 2.76$ TeV*, *JHEP* **10** (2018) 061 [arXiv:1805.04379] [INSPIRE].

[154] ALICE collaboration, *Measurement of electrons from semileptonic heavy-flavor hadron decays in pp collisions at $\sqrt{s} = 2.76$ TeV*, *Phys. Rev. D* **91** (2015) 012001 [arXiv:1405.4117] [INSPIRE].

[155] ALICE collaboration, *Inclusive heavy-flavour production at central and forward rapidity in Xe-Xe collisions at $\sqrt{s_{\rm NN}} = 5.44$ TeV*, *Phys. Lett. B* **819** (2021) 136437 [arXiv:2011.06970] [INSPIRE].

[156] C. Oleari, *The POWHEG-BOX*, *Nucl. Phys. B Proc. Suppl.* **205-206** (2010) 36 [arXiv:1007.3893] [INSPIRE].

[157] E. Fermi, *An attempt of a theory of beta radiation.* 1, *Z. Phys.* **88** (1934) 161 [INSPIRE].

[158] F.L. Wilson, *Fermi's theory of beta decay*, *Am. J. Phys.* **36** (1968) 1150 [INSPIRE].

[159] ALICE collaboration, *ALICE 2016–2017–2018 luminosity determination for pp collisions at $\sqrt{s} = 13$ TeV*, ALICE-PUBLIC-2021-005, CERN, Geneva, Switzerland (2021).

[160] ALICE collaboration, *Measurement of D-meson production at mid-rapidity in pp collisions at $\sqrt{s} = 7$ TeV*, *Eur. Phys. J. C* **77** (2017) 550 [arXiv:1702.00766] [INSPIRE].

[161] ALICE collaboration, *The ALICE definition of primary particles*, ALICE-PUBLIC-2017-005, CERN, Geneva, Switzerland (2017).

[162] P.M. Nadolsky et al., *Implications of CTEQ global analysis for collider observables*, *Phys. Rev. D* **78** (2008) 013004 [arXiv:0802.0007] [INSPIRE].

[163] STAR collaboration, *High p_T non-photonic electron production in p+p collisions at $\sqrt{s} = 200$ GeV*, *Phys. Rev. D* **83** (2011) 052006 [arXiv:1102.2611] [INSPIRE].

JHEP08(2023)006

[164] PHENIX collaboration, *Measurement of high-p_T single electrons from heavy-flavor decays in p+p collisions at $\sqrt{s} = 200$ GeV*, *Phys. Rev. Lett.* **97** (2006) 252002 [hep-ex/0609010] [INSPIRE].

[165] ALICE collaboration, *Measurement of beauty and charm production in pp collisions at $\sqrt{s} = 5.02$ TeV via non-prompt and prompt D mesons*, *JHEP* **05** (2021) 220 [arXiv:2102.13601] [INSPIRE].

[166] STAR collaboration, *Measurements of D^0 and D^* production in p+p collisions at $\sqrt{s} = 200$ GeV*, *Phys. Rev. D* **86** (2012) 072013 [arXiv:1204.4244] [INSPIRE].

[167] CDF collaboration, *Measurement of prompt charm meson production cross sections in $p\bar{p}$ collisions at $\sqrt{s} = 1.96$ TeV*, *Phys. Rev. Lett.* **91** (2003) 241804 [hep-ex/0307080] [INSPIRE].

[168] ALICE collaboration, *Charm-quark fragmentation fractions and production cross section at midrapidity in pp collisions at the LHC*, *Phys. Rev. D* **105** (2022) L011103 [arXiv:2105.06335] [INSPIRE].

[169] ALICE collaboration, *Beauty production in pp collisions at $\sqrt{s} = 2.76$ TeV measured via semi-electronic decays*, *Phys. Lett. B* **738** (2014) 97 [arXiv:1405.4144] [INSPIRE].

[170] R. Averbeck et al., *Reference heavy flavour cross sections in pp collisions at $\sqrt{s} = 2.76$ TeV, using a pQCD-driven $\sqrt{s}$-scaling of ALICE measurements at $\sqrt{s} = 7$ TeV*, arXiv:1107.3243 [INSPIRE].

[171] ALICE collaboration, *Beauty production in pp collisions at $\sqrt{s} = 2.76$ TeV measured via semi-electronic decays*, *Phys. Lett. B* **738** (2014) 97 [arXiv:1405.4144] [INSPIRE].

[172] Z.-B. Kang et al., *Multiple scattering effects on heavy meson production in p+A collisions at backward rapidity*, *Phys. Lett. B* **740** (2015) 23 [arXiv:1409.2494] [INSPIRE].

[173] S.G. Weber, A. Dubla, A. Andronic and A. Morsch, *Elucidating the multiplicity dependence of J/ψ production in proton-proton collisions with PYTHIA8*, *Eur. Phys. J. C* **79** (2019) 36 [arXiv:1811.07744] [INSPIRE].

[174] ATLAS collaboration, *A study of different colour reconnection settings for PYTHIA8 generator using underlying event observables*, ATL-PHYS-PUB-2017-008, CERN, Geneva, Switzerland (2017).

[175] J.R. Christiansen and P.Z. Skands, *String formation beyond leading colour*, *JHEP* **08** (2015) 003 [arXiv:1505.01681] [INSPIRE].

[176] K. Werner et al., *Charm production in high multiplicity pp events*, in the proceedings of the 7th *international workshop on multiple partonic interactions at the LHC*, (2016), p. 66 [arXiv:1602.03414] [INSPIRE].

[177] ALICE collaboration, *Multiplicity dependence of (multi-)strange hadron production in proton-proton collisions at $\sqrt{s} = 13$ TeV*, *Eur. Phys. J. C* **80** (2020) 167 [arXiv:1908.01861] [INSPIRE].

[178] K. Werner et al., *Event-by-event simulation of the three-dimensional hydrodynamic evolution from flux tube initial conditions in ultrarelativistic heavy ion collisions*, *Phys. Rev. C* **82** (2010) 044904 [arXiv:1004.0805] [INSPIRE].

JHEP08(2023)006

The ALICE collaboration

S. Acharya[125], D. Adamová[86], A. Adler[69], G. Aglieri Rinella[32], M. Agnello[29], N. Agrawal[50], Z. Ahammed[132], S. Ahmad[15], S.U. Ahn[70], I. Ahuja[37], A. Akindinov[140], M. Al-Turany[97], D. Aleksandrov[140], B. Alessandro[55], H.M. Alfanda[6], R. Alfaro Molina[66], B. Ali[15], A. Alici[25], N. Alizadehvandchali[114], A. Alkin[32], J. Alme[20], G. Alocco[51], T. Alt[63], I. Altsybeev[140], M.N. Anaam[6], C. Andrei[45], A. Andronic[135], V. Anguelov[94], F. Antinori[53], P. Antonioli[50], N. Apadula[74], L. Aphecetche[103], H. Appelshäuser[63], C. Arata[73], S. Arcelli[25], M. Aresti[51], R. Arnaldi[55], J.G.M.C.A. Arneiro[110], I.C. Arsene[19], M. Arslandok[137], A. Augustinus[32], R. Averbeck[97], M.D. Azmi[15], A. Badalà[52], J. Bae[104], Y.W. Baek[40], X. Bai[118], R. Bailhache[63], Y. Bailung[47], A. Balbino[29], A. Baldisseri[128], B. Balis[2], D. Banerjee[4], Z. Banoo[91], R. Barbera[26], F. Barile[31], L. Barioglio[95], M. Barlou[78], G.G. Barnaföldi[136], L.S. Barnby[85], V. Barret[125], L. Barreto[110], C. Bartels[117], K. Barth[32], E. Bartsch[63], N. Bastid[125], S. Basu[75], G. Batigne[103], D. Battistini[95], B. Batyunya[141], D. Bauri[46], J.L. Bazo Alba[101], I.G. Bearden[83], C. Beattie[137], P. Becht[97], D. Behera[47], I. Belikov[127], A.D.C. Bell Hechavarria[135], F. Bellini[25], R. Bellwied[114], S. Belokurova[140], G. Bencedi[136], S. Beole[24], A. Bercuci[45], Y. Berdnikov[140], A. Berdnikova[94], L. Bergmann[94], M.G. Besoiu[62], L. Betev[32], P.P. Bhaduri[132], A. Bhasin[91], M.A. Bhat[4], B. Bhattacharjee[41], L. Bianchi[24], N. Bianchi[48], J. Bielčík[35], J. Bielčíková[86], J. Biernat[107], A.P. Bigot[127], A. Bilandzic[95], G. Biro[136], S. Biswas[4], N. Bize[103], J.T. Blair[108], D. Blau[140], M.B. Blidaru[97], N. Bluhme[38], C. Blume[63], G. Boca[21,54], F. Bock[87], T. Bodova[20], A. Bogdanov[140], S. Boi[22], J. Bok[57], L. Boldizsár[136], M. Bombara[37], P.M. Bond[32], G. Bonomi[131,54], H. Borel[128], A. Borissov[140], A.G. Borquez Carcamo[94], H. Bossi[137], E. Botta[24], Y.E.M. Bouziani[63], L. Bratrud[63], P. Braun-Munzinger[97], M. Bregant[110], M. Broz[35], G.E. Bruno[96,31], M.D. Buckland[23], D. Budnikov[140], H. Buesching[63], S. Bufalino[29], P. Buhler[102], Z. Buthelezi[67,121], A. Bylinkin[20], S.A. Bysiak[107], M. Cai[6], H. Caines[137], A. Caliva[28], E. Calvo Villar[101], J.M.M. Camacho[109], P. Camerini[23], F.D.M. Canedo[110], M. Carabas[124], A.A. Carballo[32], F. Carnesecchi[32], R. Caron[126], L.A.D. Carvalho[110], J. Castillo Castellanos[128], F. Catalano[32,24], C. Ceballos Sanchez[141], I. Chakaberia[74], P. Chakraborty[46], S. Chandra[132], S. Chapeland[32], M. Chartier[117], S. Chattopadhyay[132], S. Chattopadhyay[99], T.G. Chavez[44], T. Cheng[97,6], C. Cheshkov[126], B. Cheynis[126], V. Chibante Barroso[32], D.D. Chinellato[111], E.S. Chizzali[II,95], J. Cho[57], S. Cho[57], P. Chochula[32], P. Christakoglou[84], C.H. Christensen[83], P. Christiansen[75], T. Chujo[123], M. Ciacco[29], C. Cicalo[51], F. Cindolo[50], M.R. Ciupek[97], G. Clai[III,50], F. Colamaria[49], J.S. Colburn[100], D. Colella[96,31], M. Colocci[25], G. Conesa Balbastre[73], Z. Conesa del Valle[72], G. Contin[23], J.G. Contreras[35], M.L. Coquet[128], T.M. Cormier[I,87], P. Cortese[130,55], M.R. Cosentino[112], F. Costa[32], S. Costanza[21,54], C. Cot[72], J. Crkovská[94], P. Crochet[125], R. Cruz-Torres[74], P. Cui[6], A. Dainese[53], M.C. Danisch[94], A. Danu[62], P. Das[80], P. Das[4], S. Das[4], A.R. Dash[135], S. Dash[46], A. De Caro[28], G. de Cataldo[49], J. de Cuveland[38], A. De Falco[22], D. De Gruttola[28], N. De Marco[55], C. De Martin[23], S. De

JHEP08(2023)006

Pasquale[28], R. Deb[131], S. Deb[47], K.R. Deja[133], R. Del Grande[95], L. Dello Stritto[28], W. Deng[6], P. Dhankher[18], D. Di Bari[31], A. Di Mauro[32], B. Diab[128], R.A. Diaz[141,7], T. Dietel[113], Y. Ding[6], R. Divià[32], D.U. Dixit[18], Ø. Djuvsland[20], U. Dmitrieva[140], A. Dobrin[62], B. Dönigus[63], J.M. Dubinski[133], A. Dubla[97], S. Dudi[90], P. Dupieux[125], M. Durkac[106], N. Dzalaiova[12], T.M. Eder[135], R.J. Ehlers[74], F. Eisenhut[63], D. Elia[49], B. Erazmus[103], F. Ercolessi[25], F. Erhardt[89], M.R. Ersdal[20], B. Espagnon[72], G. Eulisse[32], D. Evans[100], S. Evdokimov[140], L. Fabbietti[95], M. Faggin[27], J. Faivre[73], F. Fan[6], W. Fan[74], A. Fantoni[48], M. Fasel[87], P. Fecchio[29], A. Feliciello[55], G. Feofilov[140], A. Fernández Téllez[44], L. Ferrandi[110], M.B. Ferrer[32], A. Ferrero[128], C. Ferrero[55], A. Ferretti[24], V.J.G. Feuillard[94], V. Filova[35], D. Finogeev[140], F.M. Fionda[51], F. Flor[114], A.N. Flores[108], S. Foertsch[67], I. Fokin[94], S. Fokin[140], E. Fragiacomo[56], E. Frajna[136], U. Fuchs[32], N. Funicello[28], C. Furget[73], A. Furs[140], T. Fusayasu[98], J.J. Gaardhøje[83], M. Gagliardi[24], A.M. Gago[101], C.D. Galvan[109], D.R. Gangadharan[114], P. Ganoti[78], C. Garabatos[97], J.R.A. Garcia[44], E. Garcia-Solis[9], C. Gargiulo[32], A. Garibli[81], K. Garner[135], P. Gasik[97], A. Gautam[116], M.B. Gay Ducati[65], M. Germain[103], A. Ghimouz[123], C. Ghosh[132], M. Giacalone[50,25], P. Giubellino[97,55], P. Giubilato[27], A.M.C. Glaenzer[128], P. Glässel[94], E. Glimos[120], D.J.Q. Goh[76], V. Gonzalez[134], S. Gorbunov[38], M. Gorgon[2], K. Goswami[47], S. Gotovac[33], V. Grabski[66], L.K. Graczykowski[133], E. Grecka[86], A. Grelli[58], C. Grigoras[32], V. Grigoriev[140], S. Grigoryan[141,1], F. Grosa[32], J.F. Grosse-Oetringhaus[32], R. Grosso[97], D. Grund[35], G.G. Guardiano[111], R. Guernane[73], M. Guilbaud[103], K. Gulbrandsen[83], T. Gundem[63], T. Gunji[122], W. Guo[6], A. Gupta[91], R. Gupta[91], R. Gupta[47], S.P. Guzman[44], K. Gwizdziel[133], L. Gyulai[136], M.K. Habib[97], C. Hadjidakis[72], F.U. Haider[91], H. Hamagaki[76], A. Hamdi[74], M. Hamid[6], Y. Han[138], B.G. Hanley[134], R. Hannigan[108], J. Hansen[75], M.R. Haque[133], J.W. Harris[137], A. Harton[9], H. Hassan[87], D. Hatzifotiadou[50], P. Hauer[42], L.B. Havener[137], S.T. Heckel[95], E. Hellbär[97], H. Helstrup[34], M. Hemmer[63], T. Herman[35], G. Herrera Corral[8], F. Herrmann[135], S. Herrmann[126], K.F. Hetland[34], B. Heybeck[63], H. Hillemanns[32], B. Hippolyte[127], F.W. Hoffmann[69], B. Hofman[58], B. Hohlweger[84], G.H. Hong[138], M. Horst[95], A. Horzyk[2], Y. Hou[6], P. Hristov[32], C. Hughes[120], P. Huhn[63], L.M. Huhta[115], T.J. Humanic[88], A. Hutson[114], D. Hutter[38], R. Ilkaev[140], H. Ilyas[13], M. Inaba[123], G.M. Innocenti[32], M. Ippolitov[140], A. Isakov[86], T. Isidori[116], M.S. Islam[99], M. Ivanov[97], M. Ivanov[12], V. Ivanov[140], K.E. Iversen[75], M. Jablonski[2], B. Jacak[74], N. Jacazio[25], P.M. Jacobs[74], S. Jadlovska[106], J. Jadlovsky[106], S. Jaelani[82], C. Jahnke[111], M.J. Jakubowska[133], M.A. Janik[133], T. Janson[69], M. Jercic[89], S. Ji[16], S. Jia[10], A.A.P. Jimenez[64], F. Jonas[87], J.M. Jowett[32,97], J. Jung[63], M. Jung[63], A. Junique[32], A. Jusko[100], M.J. Kabus[32,133], J. Kaewjai[105], P. Kalinak[59], A.S. Kalteyer[97], A. Kalweit[32], V. Kaplin[140], A. Karasu Uysal[71], D. Karatovic[89], O. Karavichev[140], T. Karavicheva[140], P. Karczmarczyk[133], E. Karpechev[140], U. Kebschull[69], R. Keidel[139], D.L.D. Keijdener[58], M. Keil[32], B. Ketzer[42], S.S. Khade[47], A.M. Khan[118,6], S. Khan[15], A. Khanzadeev[140], Y. Kharlov[140], A. Khatun[116], A. Khuntia[107], M.B. Kidson[113], B. Kileng[34], B. Kim[104], C. Kim[16], D.J. Kim[115], E.J. Kim[68], J. Kim[138], J.S. Kim[40], J. Kim[57], J. Kim[68], M. Kim[18], S. Kim[17], T. Kim[138], K. Kimura[92], S. Kirsch[63],

JHEP08(2023)006

I. Kisel[38], S. Kiselev[140], A. Kisiel[133], J.P. Kitowski[2], J.L. Klay[5], J. Klein[32], S. Klein[74], C. Klein-Bösing[135], M. Kleiner[63], T. Klemenz[95], A. Kluge[32], A.G. Knospe[114], C. Kobdaj[105], T. Kollegger[97], A. Kondratyev[141], N. Kondratyeva[140], E. Kondratyuk[140], J. Konig[63], S.A. Konigstorfer[95], P.J. Konopka[32], G. Kornakov[133], S.D. Koryciak[2], A. Kotliarov[86], V. Kovalenko[140], M. Kowalski[107], V. Kozhuharov[36], I. Králik[59], A. Kravčáková[37], L. Krcal[32,38], M. Krivda[100,59], F. Krizek[86], K. Krizkova Gajdosova[32], M. Kroesen[94], M. Krüger[63], D.M. Krupova[35], E. Kryshen[140], V. Kučera[57], C. Kuhn[127], P.G. Kuijer[84], T. Kumaoka[123], D. Kumar[132], L. Kumar[90], N. Kumar[90], S. Kumar[31], S. Kundu[32], P. Kurashvili[79], A. Kurepin[140], A.B. Kurepin[140], A. Kuryakin[140], S. Kushpil[86], J. Kvapil[100], M.J. Kweon[57], Y. Kwon[138], S.L. La Pointe[38], P. La Rocca[26], A. Lakrathok[105], M. Lamanna[32], R. Langoy[119], P. Larionov[32], E. Laudi[32], L. Lautner[32,95], R. Lavicka[102], R. Lea[131,54], H. Lee[104], I. Legrand[45], G. Legras[135], J. Lehrbach[38], T.M. Lelek[2], R.C. Lemmon[85], I. León Monzón[109], M.M. Lesch[95], E.D. Lesser[18], P. Lévai[136], X. Li[10], X.L. Li[6], J. Lien[119], R. Lietava[100], I. Likmeta[114], B. Lim[24], S.H. Lim[16], V. Lindenstruth[38], A. Lindner[45], C. Lippmann[97], A. Liu[18], D.H. Liu[6], J. Liu[117], G.S.S. Liveraro[111], I.M. Lofnes[20], C. Loizides[87], S. Lokos[107], J. Lomker[58], P. Loncar[33], J.A. Lopez[94], X. Lopez[125], E. López Torres[7], P. Lu[97,118], J.R. Luhder[135], M. Lunardon[27], G. Luparello[56], Y.G. Ma[39], M. Mager[32], A. Maire[127], M.V. Makariev[36], M. Malaev[140], G. Malfattore[25], N.M. Malik[91], Q.W. Malik[19], S.K. Malik[91], L. Malinina[VI,141], D. Mallick[80], N. Mallick[47], G. Mandaglio[30,52], S.K. Mandal[79], V. Manko[140], F. Manso[125], V. Manzari[49], Y. Mao[6], R.W. Marcjan[2], G.V. Margagliotti[23], A. Margotti[50], A. Marín[97], C. Markert[108], P. Martinengo[32], M.I. Martínez[44], G. Martínez García[103], M.P.P. Martins[110], S. Masciocchi[97], M. Masera[24], A. Masoni[51], L. Massacrier[72], A. Mastroserio[129,49], O. Matonoha[75], S. Mattiazzo[27], P.F.T. Matuoka[110], A. Matyja[107], C. Mayer[107], A.L. Mazuecos[32], F. Mazzaschi[24], M. Mazzilli[32], J.E. Mdhluli[121], A.F. Mechler[63], Y. Melikyan[43,140], A. Menchaca-Rocha[66], E. Meninno[102,28], A.S. Menon[114], M. Meres[12], S. Mhlanga[113,67], Y. Miake[123], L. Micheletti[32], L.C. Migliorin[126], D.L. Mihaylov[95], K. Mikhaylov[141,140], A.N. Mishra[136], D. Miśkowiec[97], A. Modak[4], A.P. Mohanty[58], B. Mohanty[80], M. Mohisin Khan[IV,15], M.A. Molander[43], Z. Moravcova[83], C. Mordasini[95], D.A. Moreira De Godoy[135], I. Morozov[140], A. Morsch[32], T. Mrnjavac[32], V. Muccifora[48], S. Muhuri[132], J.D. Mulligan[74], A. Mulliri[22], M.G. Munhoz[110], R.H. Munzer[63], H. Murakami[122], S. Murray[113], L. Musa[32], J. Musinsky[59], J.W. Myrcha[133], B. Naik[121], A.I. Nambrath[18], B.K. Nandi[46], R. Nania[50], E. Nappi[49], A.F. Nassirpour[17,75], A. Nath[94], C. Nattrass[120], M.N. Naydenov[36], A. Neagu[19], A. Negru[124], L. Nellen[64], G. Neskovic[38], B.S. Nielsen[83], E.G. Nielsen[83], S. Nikolaev[140], S. Nikulin[140], V. Nikulin[140], F. Noferini[50], S. Noh[11], P. Nomokonov[141], J. Norman[117], N. Novitzky[123], P. Nowakowski[133], A. Nyanin[140], J. Nystrand[20], M. Ogino[76], A. Ohlson[75], V.A. Okorokov[140], J. Oleniacz[133], A.C. Oliveira Da Silva[120], M.H. Oliver[137], A. Onnerstad[115], C. Oppedisano[55], A. Ortiz Velasquez[64], J. Otwinowski[107], M. Oya[92], K. Oyama[76], Y. Pachmayer[94], S. Padhan[46], D. Pagano[131,54], G. Paić[64], A. Palasciano[49], S. Panebianco[128], H. Park[123], H. Park[104], J. Park[57], J.E. Parkkila[32], R.N. Patra[91], B. Paul[22], H. Pei[6],

JHEP08(2023)006

T. Peitzmann[58], X. Peng[6], M. Pennisi[24], D. Peresunko[140], G.M. Perez[7], S. Perrin[128], Y. Pestov[140], V. Petrov[140], M. Petrovici[45], R.P. Pezzi[103,65], S. Piano[56], M. Pikna[12], P. Pillot[103], O. Pinazza[50,32], L. Pinsky[114], C. Pinto[95], S. Pisano[48], M. Płoskoń[74], M. Planinic[89], F. Pliquett[63], M.G. Poghosyan[87], B. Polichtchouk[140], S. Politano[29], N. Poljak[89], A. Pop[45], S. Porteboeuf-Houssais[125], V. Pozdniakov[141], I.Y. Pozos[44], K.K. Pradhan[47], S.K. Prasad[4], S. Prasad[47], R. Preghenella[50], F. Prino[55], C.A. Pruneau[134], I. Pshenichnov[140], M. Puccio[32], S. Pucillo[24], Z. Pugelova[106], S. Qiu[84], L. Quaglia[24], R.E. Quishpe[114], S. Ragoni[14], A. Rakotozafindrabe[128], L. Ramello[130,55], F. Rami[127], S.A.R. Ramirez[44], T.A. Rancien[73], M. Rasa[26], S.S. Räsänen[43], R. Rath[50], M.P. Rauch[20], I. Ravasenga[84], K.F. Read[87,120], C. Reckziegel[112], A.R. Redelbach[38], K. Redlich[V,79], C.A. Reetz[97], A. Rehman[20], F. Reidt[32], H.A. Reme-Ness[34], Z. Rescakova[37], K. Reygers[94], A. Riabov[140], V. Riabov[140], R. Ricci[28], M. Richter[19], A.A. Riedel[95], W. Riegler[32], C. Ristea[62], S.P. Rode[141], M.V. Rodriguez[32], M. Rodríguez Cahuantzi[44], K. Røed[19], R. Rogalev[140], E. Rogochaya[141], T.S. Rogoschinski[63], D. Rohr[32], D. Röhrich[20], P.F. Rojas[44], S. Rojas Torres[35], P.S. Rokita[133], G. Romanenko[141], F. Ronchetti[48], A. Rosano[30,52], E.D. Rosas[64], K. Roslon[133], A. Rossi[53], A. Roy[47], S. Roy[46], N. Rubini[25], O.V. Rueda[114], D. Ruggiano[133], R. Rui[23], P.G. Russek[2], R. Russo[84], A. Rustamov[81], E. Ryabinkin[140], Y. Ryabov[140], A. Rybicki[107], H. Rytkonen[115], J. Ryu[16], W. Rzesa[133], O.A.M. Saarimaki[43], R. Sadek[103], S. Sadhu[31], S. Sadovsky[140], J. Saetre[20], K. Šafařík[35], P. Saha[41], S.K. Saha[4], S. Saha[80], B. Sahoo[46], B. Sahoo[47], R. Sahoo[47], S. Sahoo[60], D. Sahu[47], P.K. Sahu[60], J. Saini[132], K. Sajdakova[37], S. Sakai[123], M.P. Salvan[97], S. Sambyal[91], I. Sanna[32,95], T.B. Saramela[110], D. Sarkar[134], N. Sarkar[132], P. Sarma[41], V. Sarritzu[22], V.M. Sarti[95], M.H.P. Sas[137], J. Schambach[87], H.S. Scheid[63], C. Schiaua[45], R. Schicker[94], A. Schmah[94], C. Schmidt[97], H.R. Schmidt[93], M.O. Schmidt[32], M. Schmidt[93], N.V. Schmidt[87], A.R. Schmier[120], R. Schotter[127], A. Schröter[38], J. Schukraft[32], K. Schwarz[97], K. Schweda[97], G. Scioli[25], E. Scomparin[55], J.E. Seger[14], Y. Sekiguchi[122], D. Sekihata[122], I. Selyuzhenkov[97], S. Senyukov[127], J.J. Seo[57], D. Serebryakov[140], L. Šerkšnytė[95], A. Sevcenco[62], T.J. Shaba[67], A. Shabetai[103], R. Shahoyan[32], A. Shangaraev[140], A. Sharma[90], B. Sharma[91], D. Sharma[46], H. Sharma[53,107], M. Sharma[91], S. Sharma[76], S. Sharma[91], U. Sharma[91], A. Shatat[72], O. Sheibani[114], K. Shigaki[92], M. Shimomura[77], J. Shin[11], S. Shirinkin[140], Q. Shou[39], Y. Sibiriak[140], S. Siddhanta[51], T. Siemiarczuk[79], T.F. Silva[110], D. Silvermyr[75], T. Simantathammakul[105], R. Simeonov[36], B. Singh[91], B. Singh[95], K. Singh[47], R. Singh[80], R. Singh[91], R. Singh[47], S. Singh[15], V.K. Singh[132], V. Singhal[132], T. Sinha[99], B. Sitar[12], M. Sitta[130,55], T.B. Skaali[19], G. Skorodumovs[94], M. Slupecki[43], N. Smirnov[137], R.J.M. Snellings[58], E.H. Solheim[19], J. Song[114], A. Songmoolnak[105], C. Sonnabend[32,97], F. Soramel[27], A.B. Soto-hernandez[88], R. Spijkers[84], I. Sputowska[107], J. Staa[75], J. Stachel[94], I. Stan[62], P.J. Steffanic[120], S.F. Stiefelmaier[94], D. Stocco[103], I. Storehaug[19], P. Stratmann[135], S. Strazzi[25], C.P. Stylianidis[84], A.A.P. Suaide[110], C. Suire[72], M. Sukhanov[140], M. Suljic[32], R. Sultanov[140], V. Sumberia[91], S. Sumowidagdo[82], S. Swain[60], I. Szarka[12], M. Szymkowski[133], S.F. Taghavi[95], G. Taillepied[97], J. Takahashi[111], G.J. Tambave[80],

JHEP08(2023)006

S. Tang[6], Z. Tang[118], J.D. Tapia Takaki[116], N. Tapus[124], L.A. Tarasovicova[135], M.G. Tarzila[45], G.F. Tassielli[31], A. Tauro[32], G. Tejeda Muñoz[44], A. Telesca[32], L. Terlizzi[24], C. Terrevoli[114], S. Thakur[4], D. Thomas[108], A. Tikhonov[140], A.R. Timmins[114], M. Tkacik[106], T. Tkacik[106], A. Toia[63], R. Tokumoto[92], N. Topilskaya[140], M. Toppi[48], T. Tork[72], A.G. Torres Ramos[31], A. Trifiró[30,52], A.S. Triolo[32,30,52], S. Tripathy[50], T. Tripathy[46], S. Trogolo[32], V. Trubnikov[3], W.H. Trzaska[115], T.P. Trzcinski[133], A. Tumkin[140], R. Turrisi[53], T.S. Tveter[19], K. Ullaland[20], B. Ulukutlu[95], A. Uras[126], M. Urioni[54,131], G.L. Usai[22], M. Vala[37], N. Valle[21], L.V.R. van Doremalen[58], M. van Leeuwen[84], C.A. van Veen[94], R.J.G. van Weelden[84], P. Vande Vyvre[32], D. Varga[136], Z. Varga[136], M. Vasileiou[78], A. Vasiliev[140], O. Vázquez Doce[48], V. Vechernin[140], E. Vercellin[24], S. Vergara Limón[44], L. Vermunt[97], R. Vértesi[136], M. Verweij[58], L. Vickovic[33], Z. Vilakazi[121], O. Villalobos Baillie[100], A. Villani[23], G. Vino[49], A. Vinogradov[140], T. Virgili[28], M.M.O. Virta[115], V. Vislavicius[75], A. Vodopyanov[141], B. Volkel[32], M.A. Völkl[94], K. Voloshin[140], S.A. Voloshin[134], G. Volpe[31], B. von Haller[32], I. Vorobyev[95], N. Vozniuk[140], J. Vrláková[37], J. Wan[39], C. Wang[39], D. Wang[39], Y. Wang[39], A. Wegrzynek[32], F.T. Weiglhofer[38], S.C. Wenzel[32], J.P. Wessels[135], S.L. Weyhmiller[137], J. Wiechula[63], J. Wikne[19], G. Wilk[79], J. Wilkinson[97], G.A. Willems[135], B. Windelband[94], M. Winn[128], J.R. Wright[108], W. Wu[39], Y. Wu[118], R. Xu[6], A. Yadav[42], A.K. Yadav[132], S. Yalcin[71], Y. Yamaguchi[92], S. Yang[20], S. Yano[92], Z. Yin[6], I.-K. Yoo[16], J.H. Yoon[57], H. Yu[11], S. Yuan[20], A. Yuncu[94], V. Zaccolo[23], C. Zampolli[32], F. Zanone[94], N. Zardoshti[32], A. Zarochentsev[140], P. Závada[61], N. Zaviyalov[140], M. Zhalov[140], B. Zhang[6], L. Zhang[39], S. Zhang[39], X. Zhang[6], Y. Zhang[118], Z. Zhang[6], M. Zhao[10], V. Zherebchevskii[140], Y. Zhi[10], D. Zhou[6], Y. Zhou[83], J. Zhu[97,6], Y. Zhu[6], S.C. Zugravel[55], N. Zurlo[131,54]

[1] *A.I. Alikhanyan National Science Laboratory (Yerevan Physics Institute) Foundation, Yerevan, Armenia*
[2] *AGH University of Science and Technology, Cracow, Poland*
[3] *Bogolyubov Institute for Theoretical Physics, National Academy of Sciences of Ukraine, Kiev, Ukraine*
[4] *Bose Institute, Department of Physics and Centre for Astroparticle Physics and Space Science (CAPSS), Kolkata, India*
[5] *California Polytechnic State University, San Luis Obispo, California, United States*
[6] *Central China Normal University, Wuhan, China*
[7] *Centro de Aplicaciones Tecnológicas y Desarrollo Nuclear (CEADEN), Havana, Cuba*
[8] *Centro de Investigación y de Estudios Avanzados (CINVESTAV), Mexico City and Mérida, Mexico*
[9] *Chicago State University, Chicago, Illinois, United States*
[10] *China Institute of Atomic Energy, Beijing, China*
[11] *Chungbuk National University, Cheongju, Republic of Korea*
[12] *Comenius University Bratislava, Faculty of Mathematics, Physics and Informatics, Bratislava, Slovak Republic*
[13] *COMSATS University Islamabad, Islamabad, Pakistan*
[14] *Creighton University, Omaha, Nebraska, United States*
[15] *Department of Physics, Aligarh Muslim University, Aligarh, India*
[16] *Department of Physics, Pusan National University, Pusan, Republic of Korea*
[17] *Department of Physics, Sejong University, Seoul, Republic of Korea*
[18] *Department of Physics, University of California, Berkeley, California, United States*

JHEP08(2023)006

[19] *Department of Physics, University of Oslo, Oslo, Norway*
[20] *Department of Physics and Technology, University of Bergen, Bergen, Norway*
[21] *Dipartimento di Fisica, Università di Pavia, Pavia, Italy*
[22] *Dipartimento di Fisica dell'Università and Sezione INFN, Cagliari, Italy*
[23] *Dipartimento di Fisica dell'Università and Sezione INFN, Trieste, Italy*
[24] *Dipartimento di Fisica dell'Università and Sezione INFN, Turin, Italy*
[25] *Dipartimento di Fisica e Astronomia dell'Università and Sezione INFN, Bologna, Italy*
[26] *Dipartimento di Fisica e Astronomia dell'Università and Sezione INFN, Catania, Italy*
[27] *Dipartimento di Fisica e Astronomia dell'Università and Sezione INFN, Padova, Italy*
[28] *Dipartimento di Fisica 'E.R. Caianiello' dell'Università and Gruppo Collegato INFN, Salerno, Italy*
[29] *Dipartimento DISAT del Politecnico and Sezione INFN, Turin, Italy*
[30] *Dipartimento di Scienze MIFT, Università di Messina, Messina, Italy*
[31] *Dipartimento Interateneo di Fisica 'M. Merlin' and Sezione INFN, Bari, Italy*
[32] *European Organization for Nuclear Research (CERN), Geneva, Switzerland*
[33] *Faculty of Electrical Engineering, Mechanical Engineering and Naval Architecture, University of Split, Split, Croatia*
[34] *Faculty of Engineering and Science, Western Norway University of Applied Sciences, Bergen, Norway*
[35] *Faculty of Nuclear Sciences and Physical Engineering, Czech Technical University in Prague, Prague, Czech Republic*
[36] *Faculty of Physics, Sofia University, Sofia, Bulgaria*
[37] *Faculty of Science, P.J. Šafárik University, Košice, Slovak Republic*
[38] *Frankfurt Institute for Advanced Studies, Johann Wolfgang Goethe-Universität Frankfurt, Frankfurt, Germany*
[39] *Fudan University, Shanghai, China*
[40] *Gangneung-Wonju National University, Gangneung, Republic of Korea*
[41] *Gauhati University, Department of Physics, Guwahati, India*
[42] *Helmholtz-Institut für Strahlen- und Kernphysik, Rheinische Friedrich-Wilhelms-Universität Bonn, Bonn, Germany*
[43] *Helsinki Institute of Physics (HIP), Helsinki, Finland*
[44] *High Energy Physics Group, Universidad Autónoma de Puebla, Puebla, Mexico*
[45] *Horia Hulubei National Institute of Physics and Nuclear Engineering, Bucharest, Romania*
[46] *Indian Institute of Technology Bombay (IIT), Mumbai, India*
[47] *Indian Institute of Technology Indore, Indore, India*
[48] *INFN, Laboratori Nazionali di Frascati, Frascati, Italy*
[49] *INFN, Sezione di Bari, Bari, Italy*
[50] *INFN, Sezione di Bologna, Bologna, Italy*
[51] *INFN, Sezione di Cagliari, Cagliari, Italy*
[52] *INFN, Sezione di Catania, Catania, Italy*
[53] *INFN, Sezione di Padova, Padova, Italy*
[54] *INFN, Sezione di Pavia, Pavia, Italy*
[55] *INFN, Sezione di Torino, Turin, Italy*
[56] *INFN, Sezione di Trieste, Trieste, Italy*
[57] *Inha University, Incheon, Republic of Korea*
[58] *Institute for Gravitational and Subatomic Physics (GRASP), Utrecht University/Nikhef, Utrecht, Netherlands*
[59] *Institute of Experimental Physics, Slovak Academy of Sciences, Košice, Slovak Republic*
[60] *Institute of Physics, Homi Bhabha National Institute, Bhubaneswar, India*
[61] *Institute of Physics of the Czech Academy of Sciences, Prague, Czech Republic*
[62] *Institute of Space Science (ISS), Bucharest, Romania*
[63] *Institut für Kernphysik, Johann Wolfgang Goethe-Universität Frankfurt, Frankfurt, Germany*
[64] *Instituto de Ciencias Nucleares, Universidad Nacional Autónoma de México, Mexico City, Mexico*
[65] *Instituto de Física, Universidade Federal do Rio Grande do Sul (UFRGS), Porto Alegre, Brazil*

JHEP08(2023)006

[66] Instituto de Física, Universidad Nacional Autónoma de México, Mexico City, Mexico
[67] iThemba LABS, National Research Foundation, Somerset West, South Africa
[68] Jeonbuk National University, Jeonju, Republic of Korea
[69] Johann-Wolfgang-Goethe Universität Frankfurt Institut für Informatik, Fachbereich Informatik und Mathematik, Frankfurt, Germany
[70] Korea Institute of Science and Technology Information, Daejeon, Republic of Korea
[71] KTO Karatay University, Konya, Turkey
[72] Laboratoire de Physique des 2 Infinis, Irène Joliot-Curie, Orsay, France
[73] Laboratoire de Physique Subatomique et de Cosmologie, Université Grenoble-Alpes, CNRS-IN2P3, Grenoble, France
[74] Lawrence Berkeley National Laboratory, Berkeley, California, United States
[75] Lund University Department of Physics, Division of Particle Physics, Lund, Sweden
[76] Nagasaki Institute of Applied Science, Nagasaki, Japan
[77] Nara Women's University (NWU), Nara, Japan
[78] National and Kapodistrian University of Athens, School of Science, Department of Physics, Athens, Greece
[79] National Centre for Nuclear Research, Warsaw, Poland
[80] National Institute of Science Education and Research, Homi Bhabha National Institute, Jatni, India
[81] National Nuclear Research Center, Baku, Azerbaijan
[82] National Research and Innovation Agency — BRIN, Jakarta, Indonesia
[83] Niels Bohr Institute, University of Copenhagen, Copenhagen, Denmark
[84] Nikhef, National institute for subatomic physics, Amsterdam, Netherlands
[85] Nuclear Physics Group, STFC Daresbury Laboratory, Daresbury, United Kingdom
[86] Nuclear Physics Institute of the Czech Academy of Sciences, Husinec-Řež, Czech Republic
[87] Oak Ridge National Laboratory, Oak Ridge, Tennessee, United States
[88] Ohio State University, Columbus, Ohio, United States
[89] Physics department, Faculty of science, University of Zagreb, Zagreb, Croatia
[90] Physics Department, Panjab University, Chandigarh, India
[91] Physics Department, University of Jammu, Jammu, India
[92] Physics Program and International Institute for Sustainability with Knotted Chiral Meta Matter (SKCM2), Hiroshima University, Hiroshima, Japan
[93] Physikalisches Institut, Eberhard-Karls-Universität Tübingen, Tübingen, Germany
[94] Physikalisches Institut, Ruprecht-Karls-Universität Heidelberg, Heidelberg, Germany
[95] Physik Department, Technische Universität München, Munich, Germany
[96] Politecnico di Bari and Sezione INFN, Bari, Italy
[97] Research Division and ExtreMe Matter Institute EMMI, GSI Helmholtzzentrum für Schwerionenforschung GmbH, Darmstadt, Germany
[98] Saga University, Saga, Japan
[99] Saha Institute of Nuclear Physics, Homi Bhabha National Institute, Kolkata, India
[100] School of Physics and Astronomy, University of Birmingham, Birmingham, United Kingdom
[101] Sección Física, Departamento de Ciencias, Pontificia Universidad Católica del Perú, Lima, Peru
[102] Stefan Meyer Institut für Subatomare Physik (SMI), Vienna, Austria
[103] SUBATECH, IMT Atlantique, Nantes Université, CNRS-IN2P3, Nantes, France
[104] Sungkyunkwan University, Suwon City, Republic of Korea
[105] Suranaree University of Technology, Nakhon Ratchasima, Thailand
[106] Technical University of Košice, Košice, Slovak Republic
[107] The Henryk Niewodniczanski Institute of Nuclear Physics, Polish Academy of Sciences, Cracow, Poland
[108] The University of Texas at Austin, Austin, Texas, United States
[109] Universidad Autónoma de Sinaloa, Culiacán, Mexico
[110] Universidade de São Paulo (USP), São Paulo, Brazil
[111] Universidade Estadual de Campinas (UNICAMP), Campinas, Brazil

JHEP08(2023)006

[112] Universidade Federal do ABC, Santo Andre, Brazil
[113] University of Cape Town, Cape Town, South Africa
[114] University of Houston, Houston, Texas, United States
[115] University of Jyväskylä, Jyväskylä, Finland
[116] University of Kansas, Lawrence, Kansas, United States
[117] University of Liverpool, Liverpool, United Kingdom
[118] University of Science and Technology of China, Hefei, China
[119] University of South-Eastern Norway, Kongsberg, Norway
[120] University of Tennessee, Knoxville, Tennessee, United States
[121] University of the Witwatersrand, Johannesburg, South Africa
[122] University of Tokyo, Tokyo, Japan
[123] University of Tsukuba, Tsukuba, Japan
[124] University Politehnica of Bucharest, Bucharest, Romania
[125] Université Clermont Auvergne, CNRS/IN2P3, LPC, Clermont-Ferrand, France
[126] Université de Lyon, CNRS/IN2P3, Institut de Physique des 2 Infinis de Lyon, Lyon, France
[127] Université de Strasbourg, CNRS, IPHC UMR 7178, F-67000 Strasbourg, France, Strasbourg, France
[128] Université Paris-Saclay Centre d'Etudes de Saclay (CEA), IRFU, Départment de Physique Nucléaire (DPhN), Saclay, France
[129] Università degli Studi di Foggia, Foggia, Italy
[130] Università del Piemonte Orientale, Vercelli, Italy
[131] Università di Brescia, Brescia, Italy
[132] Variable Energy Cyclotron Centre, Homi Bhabha National Institute, Kolkata, India
[133] Warsaw University of Technology, Warsaw, Poland
[134] Wayne State University, Detroit, Michigan, United States
[135] Westfälische Wilhelms-Universität Münster, Institut für Kernphysik, Münster, Germany
[136] Wigner Research Centre for Physics, Budapest, Hungary
[137] Yale University, New Haven, Connecticut, United States
[138] Yonsei University, Seoul, Republic of Korea
[139] Zentrum für Technologie und Transfer (ZTT), Worms, Germany
[140] Affiliated with an institute covered by a cooperation agreement with CERN
[141] Affiliated with an international laboratory covered by a cooperation agreement with CERN

[I] Deceased
[II] Also at: Max-Planck-Institut für Physik, Munich, Germany
[III] Also at: Italian National Agency for New Technologies, Energy and Sustainable Economic Development (ENEA), Bologna, Italy
[IV] Also at: Department of Applied Physics, Aligarh Muslim University, Aligarh, India
[V] Also at: Institute of Theoretical Physics, University of Wroclaw, Poland
[VI] Also at: An institution covered by a cooperation agreement with CERN

JHEP08(2023)006